A THESIS

FOR THE DEGREE OF MASTER OF SCIENCE

Anti-inflammatory and anti-melanogenic effects of Pinostrobin

ATHAPATHTHU MUDIYANSELAGE GIHAN KAVINDA ATHAPATHTHU

Department of Marine Life Sciences

SCHOOL OF BIOMEDICAL SCIENCE

JEJU NATIONAL UNIVERSITY

REPUBLIC OF KOREA

AUGUST 2022

Anti-inflammatory and anti-melanogenic effects of pinostrobin

Athapaththu Mudiyanselage Gihan Kavinda Athapaththu

(Supervised by Professor Gi-Young Kim)

A thesis submitted in partial fulfillment of the requirement for the degree of masters

August 2022

The thesis has been examined and approved by

…….
Sang Rul Park, Professor of Jeju National University

…….
Seung Heon Lee, Professor of Jeju National University

……..
Gi-Young Kim, Professor of Jeju National University

August 2022

Date

Department of Marine Life Science

GRADUATE SCHOOL

JEJU NATIONAL UNIVERSITY

Acknowledgments

First of all, I have to say, even though this is an individual work, it could never be researched the heights without the support, guidance, and efforts lot of people. First and foremost, I would like to express my sincere gratitude to my supervisor Prof. Gi-Young Kim, who has supported me throughout this period with his patience and knowledge whilst allowing me the room to work in my way. I attribute the level of my master's degree to his effort and encouragement. Without the guidance of Prof. Gi-Young Kim, this thesis, too, would not have been completed or written.

Then, I would like to thank all my lab members, especially Dr. Neelaka Molagoda, Dr. Sung Young Kang, Mr. Hasitha Karunarathne, Mr. Chanaka Jayasinghe, and Mr. Dumindu Kavinda for their encouragement, valuable comments, and helping me to be successful in my research throughout this challenging period. I also express my gratitude to Prof. U.P.K. Epa, my former supervisor and Prof. Devika M. de Costa for introducing me to Prof. Gi-Young Kim. Also, my family members and friends especially my wife Manasee Weerathunga for standing beside me throughout this wonderful journey.

However, I am the only person responsible for any error in the thesis and all the comments on this are highly appreciated.

Table of Content

List of Figures

List of Tables

PART 01

Pinostrobin ameliorates lipopolysaccharide (LPS)-induced inflammation and endotoxemia by inhibiting LPS binding to the TLR4/MD2 complex

Abstract

Pinostrobin is a natural flavonoid with valuable pharmacological properties, including anti-cancer, anti-viral, and anti-oxidant activities. However, the anti-inflammatory effects of pinostrobin have not been well studied. In this study, we investigated whether pinostrobin attenuates lipopolysaccharide (LPS)-induced inflammation and endotoxemia. Additionally, the target molecule of pinostrobin was identified through molecular docking simulation. Pinostrobin decreased LPS-induced nitric oxide (NO) and prostaglandin E_2 production and reduced the expression of inducible NO synthase and cyclooxygenase-2. Furthermore, pinostrobin inhibited the production of proinflammatory cytokines, including interleukin-12 and tumor necrosis factor-α in LPS-stimulated RAW 264.7 macrophages accompanied by inhibiting nuclear translocation of nuclear factor-κB (NF-κB). The anti-inflammatory effect of pinostrobin was further confirmed in LPS-microinjected zebrafish larvae by diminishing the recruitment of macrophages and neutrophils, and proinflammatory gene expression. Moreover, LPS-microinjected zebrafish larvae showed a decrease in heart rate and an increase in mortality and abnormalities. However, pinostrobin significantly attenuated these adverse effects. Molecular docking showed that pinostrobin fits into myeloid differentiation factor (MD2) and Toll-like receptor 4 (TLR4) with no traditional hydrogen bonds (pose 1). The 2D ligand interaction diagram showed that pinostrobin forms a carbon hydrogen bond with LYS89 in MD2 and many non-covalent interactions, including π-alkyl or alkyl and van der Waals interactions, indicating that pinostrobin hinders LPS binding between MD2 and TLR4 and consequently inhibits TLR4/MD2-mediated inflammatory responses. These data suggest that pinostrobin attenuates LPS-induced inflammation and endotoxemia by binding to the TLR4/MD2 complex.

Key words: Pinostrobin; Inflammation; Toll-like receptor 4; Myeloid differentiation factor 2; Nuclear factor-κB

1. Introduction

Inflammation is a highly regulated self-limiting process for detecting and destroying invading pathogens and restoring normal tissue structure and function [1]. Once pathogens such as bacteria, invade, blood monocytes rapidly migrate to the site of infection through interaction with vascular endothelial cells, followed by full differentiation into tissue macrophages [2]. Macrophages immediately initiate and enhance inflammatory responses by releasing proinflammatory cytokines, including interleukin-12 (IL-12) and tumor necrosis factor-α (TNF-α), and proinflammatory mediators, including nitric oxide (NO) and prostaglandin E_2 (PGE_2) [3], which eliminate pathogens by activating innate immune cells. However, exaggerated and/or prolonged inflammatory responses have been recognized as major causes of chronic inflammation, including vascular disease, rheumatoid arthritis, inflammatory bowel disease, and cancers [4, 5]. Therefore, many natural compounds that inhibit the induction of inflammatory cytokines and mediators have been developed to treat inflammatory diseases.

Lipopolysaccharide (LPS), a major component of the outer membrane of gram–negative bacteria, potently triggers macrophages and neutrophils to produce proinflammatory cytokines and mediators [6, 7]. LPS micelles are first detected by soluble LPS-binding proteins and CD14, and a single LPS molecule subsequently is transferred to the Toll-like receptor 4 (TLR4) and myeloid differentiation factor (MD2) complex [8, 9]. Upon LPS binding into the TLR4/MD2 complex, intracellular Toll-IL-1 receptor (TIR) domains summon key adaptor molecules, including myeloid differentiation primary response 88 (MyD88), which stimulates inflammatory responses, and TIR-domain-containing adaptor protein inducing interferon-β mediated transcription factor (TRIF), which activates anti-viral activity [10]. Furthermore,

MyD88 promotes recruitment of IL-1 receptor-associated kinase 4 (IRAK4), which phosphorylates the IκB kinase (IKK) complex and activates nuclear factor-κB (NF-κB) through IκB degradation [11, 12]. Free NF-κB then moves into the nucleus and promotes the transcription of numerous genes involved in inflammation [13, 14]. Therefore, various antagonists targeting TLR4 and NF-κB have been developed as therapeutic agents for the treatment of LPS-induced inflammatory diseases [15].

Flavonoids are polyphenolic compounds mainly present in plants as secondary metabolites, and have been used as functional supplements because of their health benefits [16]. Pinostrobin (5-hydroxy-7-methoxy flavanone) is a natural flavonoid found in the leaves of *Cajanus cajan* (L.) Millsp. [17], and the rhizomes of *Boesenbergia rotunda* (L.) Mansf. [18] and Prunus spp. [19]. In particular, the various pharmacological effects of pinostrobin, such as anti-cancer, anti-oxidant, and neuroprotective effects, are well known [20]. Recently, Pobłocka-Olech et al. [21] also reported the anti-inflammatory and anti-oxidative effects of pinostrobin in silver nanoparticle-treated fibroblasts, and Patel et al. [22] demonstrated that pinostrobin inhibits LPS-induced TNF-α and IL-1β expression both in vitro and in vivo. Nevertheless, studies on the inhibitory effects of pinostrobin on LPS-induced inflammation are not well known.

In this study, we investigated whether pinostrobin suppresses LPS-induced inflammation and endotoxemia. Furthermore, we studied how pinostrobin inhibits the LPS-induced TLR4/MD2 signaling pathway using molecular docking.

2. Materials and methods

2.1. Reagents and antibodies

Dulbecco's modified Eagle's medium (DMEM), fetal bovine serum (FBS), trypsin-ethylenediaminetetraacetic acid (EDTA), and an antibiotic mixture were purchased from WelGENE (Daegu, Republic of Korea). LPS from *Escherichia coli* O55:B5, 3-(4,5- dimethylthiazol-2-yl)-2,5-diphenyltetrazolium bromide (MTT), methylene blue, 4′6-diamidine-2′-phenylindole dihydrochloride (DAPI), and Alexa Fluor 647 were purchased from Sigma-Aldrich (St. Louis, MO, USA). Antibodies against iNOS (sc-7271), COX-2 (sc-19999), p50 (sc-8414), p65 (sc-8008), β-actin (sc-69879), nucleolin (sc-13057), and peroxidase-labeled anti-mouse antibody (sc-16102) were purchased from Santa Cruz Biotechnology (Dallas, TX, USA). Peroxidase-labeled anti-rabbit antibodies were purchased from Koma Biotechnology (Seoul, Republic of Korea). Pinostrobin (Fig. 1A, purit: > 99%) was purified from the stems of *Prunus serrulata* Lindl. f. *serrulata spontanea* (Maxim.) Chin S. Chang and was supplied by the National Institute of Forest Science (Suwon, Gyeonggi-do, Republic of Korea). All other chemicals were purchased from Sigma-Aldrich.

2.2. Cell culture and viability

RAW 264.7 macrophages were obtained from American Type Culture Collection (Manassas, VA, USA) and cultured in DMEM supplemented with 5% FBS at 37℃ in a 5% CO_2 humidified incubator. For the analysis of relative cell viability, RAW 264.7 macrophages were seeded at a density of 1×10^5 cells/mL in 24-well plates and treated with pinostrobin (0–40 μM) 2 h before treatment with 300 ng/mL LPS for 24 h. After incubation, the colorimetric MTT assay was performed. Briefly, cells were treated with MTT solution (0.5 mg/mL) for 30 min at 37℃. Dark purple formazan was solubilized in dimethyl sulfoxide, and absorbance was measured at 540 nm using a microplate

reader (Thermo Fisher Scientific, Rockford, IL, USA).

2.3. Flow cytometric analysis

RAW 264.7 macrophages were seeded at a density of 1×10^5 cells/mL and treated with the indicated concentrations of pinostrobin (0–40 μM) for 2 h, followed by treatment with 300 ng/mL LPS for 24 h. To estimate total cell counts and dead cell population, the harvested cells were washed with ice-cold phosphate-buffered saline (PBS) and stained for 5 min with a Muse Cell Count and Viability Kit (Luminex, Austin, Texas, USA). Viable cell counts and dead cell population were measured using a Muse Cell Analyzer (Luminex).

2.4. Isolation of total RNA and reverse transcriptase-polymerase chain reactions (RT-PCR)

Total RNA was extracted from RAW 264.7 macrophages using an easy-BLUE Total RNA Extraction Kit (iNtRON Biotechnology, Seongnam, Gyeonggi-do, Republic of Korea) according to the manufacturer's instructions. RNA was reverse transcribed using moloney murine leukemia virus (MMLV) reverse transcriptase (Bioneer, Daejeon, Republic of Korea), and synthesized cDNA was amplified using EzWay Neo Taq PCR MasterMix (Koma Biotechnology) with specific primers (Table 1) [23]. *GAPDH* was used as a loading control to evaluate the relative expression of *iNOS*, *COX-2*, *IL-12*, and *TNF-α*.

Table 1. Primer sequence and PCR conditions for RAW 264.7 macrophage.

Gene*	Primer sequence (5′-3′)	Size	T_m	Cycle No.
iNOS	F: 5′-CCTCCTCCACCCTACCAAGT-3′ R: 5′-CACCCAAAGTGCTTCAGTCA-3′	199 bp	55℃	25
COX-2	F: 5′-TGCTGTACCAGCAGTGGCAA-3′ R: 5′-GCAGCCATTTCCTTCTCT CC-3′	141 bp	55℃	25
TNF-α	F: 5′-ATGAGCACAGAAAGCATGAT-3′ R: 5′-TACAGGCTTGTCACTCGAAT-3′	276 bp	53℃	25
IL-12	F: 5′-AAGACATCACACGGGACCAA-3′ R: 5′-CGCAGAGTCTCGCCATTATG-3′	318 bp	61℃	25
GAPDH	R: 5′-AGGTCGGTGTGAACGGATTTG-3′ R: 5′-TGTAGACCATGTAGTTGAGGTCA-3′	123 bp	63℃	23

Bp, base pair; T_m, melting temperature.

2.5. Western blotting

Total cell extracts were prepared from RAW 264.7 macrophages, using a radioimmunoprecipitation assay lysis buffer (iNtRON Biotechnology) with a protease inhibitor cocktail (Sigma-Aldrich). Briefly, a lysis buffer was added to the cells on ice for 30 min. In parallel, cytoplasmic, and nuclear extracts were prepared using NE-PER nuclear and cytosolic extraction reagents (Pierce, Rockford, IL, USA). Lysates were centrifuged at 15,000 × g at 4℃ for 10 min, and protein concentrations were quantified using Bio-Rad Protein Assay Reagents (Bio-Rad, Hercules, CA, USA). The samples were stored at -80°C or immediately used for western blotting. Equal amounts of protein were separated on SDS-polyacrylamide gels and transferred onto polyvinylidene fluoride membranes (Thermo Fisher Scientific). Each protein was detected using enhanced chemiluminescence (Thermo Fisher Scientific).

2.6. NO assay

RAW 264.7 macrophages (1×10^5 cells/mL) were seeded onto 24-well plates. Cells were pretreated with pinostrobin (0–20 μM) for 2 h followed by stimulation with 300 ng/mL LPS for 24 h. NO levels in the culture supernatants were determined using the Griess reagent assay. Briefly, supernatants were mixed with an equal volume of Griess reagent (1% sulfanilamide in 5% phosphoric acid and 0.1% naphthylethylenediamine dihydrochloride) and incubated in the dark at room temperature for 15 min. Absorbance was measured at 540 nm using a microplate reader (Thermo Fisher Scientific). A standard curve of sodium nitrite was used to determine nitrite concentration.

2.7. Enzyme-linked immunosorbent assay (ELISA)

ELISA was performed to quantify the secretory levels of PGE_2 (Cayman Chemicals, Ann Arbor, MI, USA), IL-12 (R&D Systems, Minneapolis, MN, USA), and TNF-α (R&D Systems) according to the manufacturer's instructions. Briefly, RAW 264.7 macrophages (1×10^5 cells/mL) were cultured in 24-well plates and pretreated with pinostrobin (0–20 μM) 2 h before adding 300 ng/ml LPS for 24 h. Supernatants were collected, and the levels of PGE_2, IL-12, and TNF-α were measured using ELISA.

2.8. Immunofluorescence staining

RAW 264.7 macrophages were cultured at a density of 1×10^4 cells/mL on 3% gelatine-coated coverslips and treated with 20 μM pinostrobin for 2 h followed by stimulation with 300 ng/mL LPS for 1 h. Cells were fixed with 4% paraformaldehyde for 10 min at 37℃ and permeabilized with 0.1% Triton X-100 for 10 min at room temperature. The cells were washed with ice-cold PBST for 5 min, blocked with 10% donkey serum for 1 h, and incubated with p65 antibody (200 μg/mL, 1:100 dilutions in 10% donkey serum) at 4℃ overnight. The cells were then washed with ice-cold PBST and incubated with a secondary antibody conjugated with Alexa Fluor 647 for 2 h at

room temperature. Finally, the cells were counterstained with the nuclear staining dye DAPI (300 nM) for 10 min. The coverslips were mounted onto glass slides using aqueous mounting medium (DAKO, Carpinteria, CA, USA). Finally, immunofluorescence was visualized using a CELENA S Digital Imaging System (Logos Biosystems, Anyang, Gyeonggi-do, Republic of Korea).

2.9. Molecular docking

The crystal structure of the TLR4/MD2 complex (PDB ID: 3FX1) was obtained from the RCSB protein database bank (PDB), and the chemical structure of pinostrobin was obtained from PubChem (https://pubchem.ncbi.nlm.nih.gov). Molecular docking was calculated using Mcule [24], and the interaction modes were visualized using UCSF Chimera [25]. 2D diagram interaction were visualized using the BIOVIA Discovery Studio Visualizer (https://discover.3ds.com).

2.10. Maintenance of zebrafish

The zebrafish study was approved by the Animal Care and Use Committee of Jeju National University (Jeju Special Self-governing Province, Republic of Korea) and carried out following the approved guidelines (approval No. 2022-0021). Zebrafish were handled as described previously [26]. Embryos were collected using natural spawning and cultured in embryo medium [(NaCl-34.8 g, KCl-1.6 g, $CaCl_2.2H_2O$-5.8 g, $MgCl_2.6H_2O$-9.78 g) with double-distilled water, pH 7.2] supplemented with 1% methylene blue at 28℃.

2.11. Heart rate, abnormality, and mortality in LPS-microinjected zebrafish larvae

Zebrafish larvae at three days post-fertilization (dpf, n=20 per group) were anesthetized using 0.002% tricaine, and 2 nL of 0.5 mg/mL LPS was microinjected into the yolk sac using a Drummond NANOJECT III injector (Drummond Scientific,

Broomall, PA). An equal volume of PBS (2 nL) was injected into the untreated control. The larvae were then transferred to 3 mL of embryo medium in the presence or absence of pinostrobin (0–20 μM). After 24 h (at 4 dpf), the heart rate was manually calculated per min. In a parallel experiment, mortality and abnormalities were measured at 5 dpf using a stereomicroscope (Olympus, Tokyo, Japan).

2.12. Macrophage and neutrophil staining in LPS-microinjected zebrafish

LPS (2 nL of 0.5 mg/mL) was microinjected into the yolk sac of 3 dpf zebrafish larvae followed by treatment with pinostrobin (0–20 μM). After 24 h (4 dpf), whole larvae were fixed with 4% methanol-free paraformaldehyde in phosphate-buffered saline (PBS) for 2 h at room temperature and rinsed in PBS. Macrophages in the larvae were stained with 5 μg/mL neutral red solution for 6 h [27]. In a parallel experiment, neutrophils in the larvae were stained with Sudan black as previously described [28]. The larvae were then washed with 70% ethanol in a water series and progressively rehydrated with 0.1% Tween in PBS. Recruitment of neutrophils and macrophages into the inflammatory sites was observed using stereomicroscopy (Olympus).

2.13. Isolation of total zebrafish mRNA and RT- PCR

Zebrafish larvae at 3 dpf were microinjected with LPS (2 nL, 0.5 mg/mL) in the yolk sac followed by treatment with pinostrobin (0–20 μM). Total RNA was extracted at 4 dpf using an Easy-BLUE Total RNA Extraction Kit (iNtRON Biotechnology), according to the manufacturer's instructions. RNA was reverse transcribed using MMLV reverse transcriptase (Bioneer). cDNA was amplified using specific primers (Table 2) [23]. *β-Actin* was used as the loading control to evaluate the relative expression of *iNOS*, *COX-2a*, *IL-12*, and *TNF-α*.

Table 2. Primer sequences and PCR conditions for zebrafish.

Gene*	Primer sequence (5′-3′)	Size	T_m	Cycle No.
iNOS	F: 5′-GGAGATGCAAGGTCAGCTTC-3′ R: 5′-GGCAAAGCTCAGTGACTTCC-3′	137 bp	58℃	27
COX-2a	F: 5′-CCTGTTGTCAAGGTCCCATT-3′ R: 5′-TCAGGGATGAACTGCTTCCT-3′	201 bp	57℃	32
TNF-α	F: 5′-TAGAACAACCCAGCAAAC-3′ R: 5′-ACCAGCGGTAAAGGCAAC-3′	149 bp	57℃	32
IL-12	F: 5′-TCTAACTTCAGCGCAGTGGA-3′ R: 5′-TGCGGTGGTGTAGTGAGTG-3′	313 bp	58℃	27
β-actin	F: 5′-CGAGCGTGGCTACAGCTTCA-3′ R: 5′-GACCGTCAGGCAGCTCATAG-3′	155 bp	61℃	27

Bp, base pair; T_m; melting temperature.

2.14. Statistical analysis

RT-PCR and western blots images were visualized using ImageQuant LAS 500 (GE healthcare Bio-Science AB, Uppsala, Sweden) and quantified using ImageJ 1.50i (National Institute of Health, Manassas, VA, USA; www.imagej.net). All data represent the mean of at least three independent experiments and are expressed as mean ± standard error (SE). Statistical analysis was performed using SigmaPlot 12.0 version (Systat Software, San Jose, CA, USA, www.systatsofware.com) by Student's *t*-test and unpaired one-way analysis of variance with the Bonferroni correction. Statistical significance was set at *, $p < 0.05$, **, $p < 0.05$, and ***, $^{\&\&\&}$, and $^{\#\#\#}$, $p < 0.001$.

3. Results

3.1. Pinostrobin at concentrations less than 20 μM is not toxic to RAW 264.7 macrophages

To investigate whether pinostrobin affects the viability of RAW 264.7 macrophages, MTT assay and flow cytometric analysis were performed. Pinostrobin at concentrations less than 20 μM did not show a significant decrease in relative cell viability, but 40 μM pinostrobin noticeably reduced the viability regardless of the presence or absence of LPS (Fig. 1B). An apparent decrease in relative cell viability was confirmed even with LPS treatment alone, because RAW 264.7 macrophages were activated and fully differentiated by LPS. Morphological changes in RAW 264.7 macrophages were not observed with pinostrobin at concentrations below 20 μM (Fig. 1C). However, at a concentration of 40 μM pinostrobin, some floating and shrunk RAW 264.7 macrophages were observed. To accurately measure the effect of pinostrobin on cell viability, a flow cytometric analysis was performed (Fig. 1D). As shown in Fig. 1E, pinostrobin slightly decreased the total viable cell count regardless of the presence of LPS, and LPS alone significantly downregulated the viable cell count compared to that in untreated cells. Although pinostrobin decreased the viable cell count in a concentration-dependent manner, it did not induce significant cell death at concentrations less than 20 μM (Fig. 1F). However, 40 μM pinostrobin significantly induced cell death. These data indicate that pinostrobin at concentrations of 20 μM or less is not toxic in RAW 264.7 macrophages.

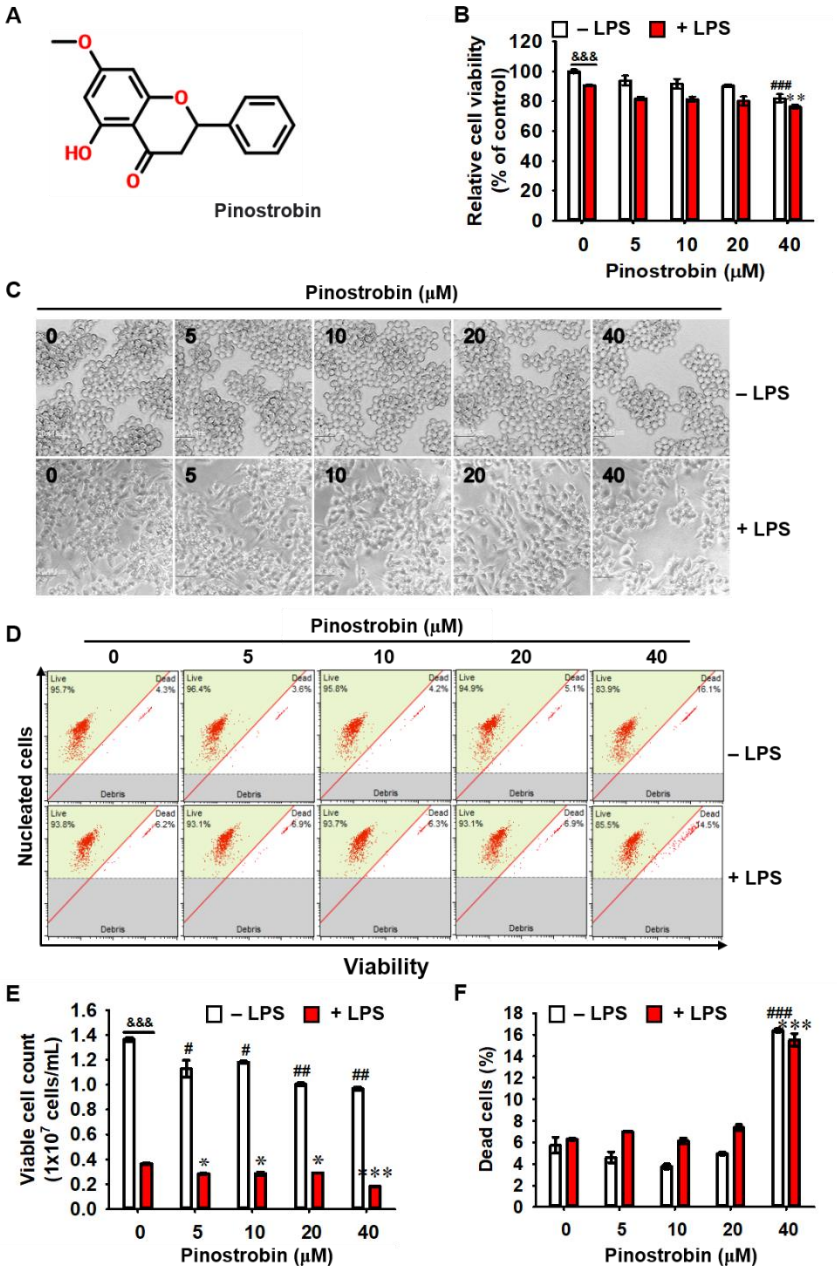

Fig. 1. Pinostrobin at concentrations of less than 20 μM does not show cytotoxicity. (A) Chemical structure of pinostrobin. (B-F) RAW264.7 macrophages were treated with 0–40 μM pinostrobin for 2 h followed by stimulation with 300 ng/mL LPS for 24 h. (B) Cell viability was determined by MTT assay. (B) Morphological images were captured under stereomicroscopy. (C) Cell viability was measured using flow cytometry. (D) Viable cell count and (E) dead cell population were obtained from flow cytometric analysis. Data are represented as the mean ± SE of three independent experiments

(*n*=3). $^{\&\&\&}$, $p < 0.001$ vs. untreated cells (Student's *t*-test); $^{\#}$, $p < 0.05$, $^{\#\#}$, $p < 0.01$, and $^{\#\#\#}$, $p < 0.001$ vs. untreated cells (One-way ANOVA); *, $p < 0.05$ and ***, $p < 0.001$ vs. LPS-treated cells (One-way ANOVA).

3.2. Pinostrobin inhibits NO and PGE_2 release along with downregulation of iNOS and COX-2 expression in LPS-stimulated RAW 264.7 macrophages

To assess the anti-inflammatory effects of pinostrobin in LPS-stimulated RAW 264.7 macrophages, we examined the levels of NO and PGE_2 released into the culture medium using Griess reagent assay and ELISA, respectively. The untreated RAW 264.7 macrophages spontaneously released the low levels of NO (1.4 ± 0.1 μM); however, LPS alone treatment significantly enhanced the levels of NO production (25.8 ± 0.7 μM; Fig. 2A). Pinostrobin treatment decreased the LPS-induced NO release in a dose-dependent manner (15.4 ± 1.4 μM, 9.6 ± 0.3 μM, and 2.8 ± 2.0 μM at 5, 10, and 20 μM, respectively). In addition, Fig. 2B showed that stimulation of RAW 264.7 macrophages with LPS results in a significant increase in PGE_2 production (2279.1 ± 50.2 pg/mL) compared to that in the untreated RAW 264.7 macrophages (543.1 ± 5.6 pg/mL). Pretreatment with pinostrobin significantly attenuated LPS-stimulated PGE_2 production in a concentration-dependent manner (1796.4 ± 12.0 pg/mL, 1505.9 ± 7.4 pg/mL, and 1403.4 ± 38.1 pg/mL at 5, 10, and 20 μM, respectively). Next, we examined whether pinostrobin affected LPS-induced iNOS and COX-2 expression at the transcriptional and translational levels. RT-PCR analysis showed a significant increase in *iNOS* and *COX-2* expression after LPS treatment, but pretreatment with pinostrobin attenuated this expression in a concentration-dependent manner (Fig. 2C). Consistent with RT-PCR data, pinostrobin noticeably inhibited LPS-induced iNOS and COX-2 expression at the translational level (Fig. 2D). These data indicated that pinostrobin suppressed LPS-stimulated NO and PGE_2 release by inhibiting iNOS and COX-2 expression.

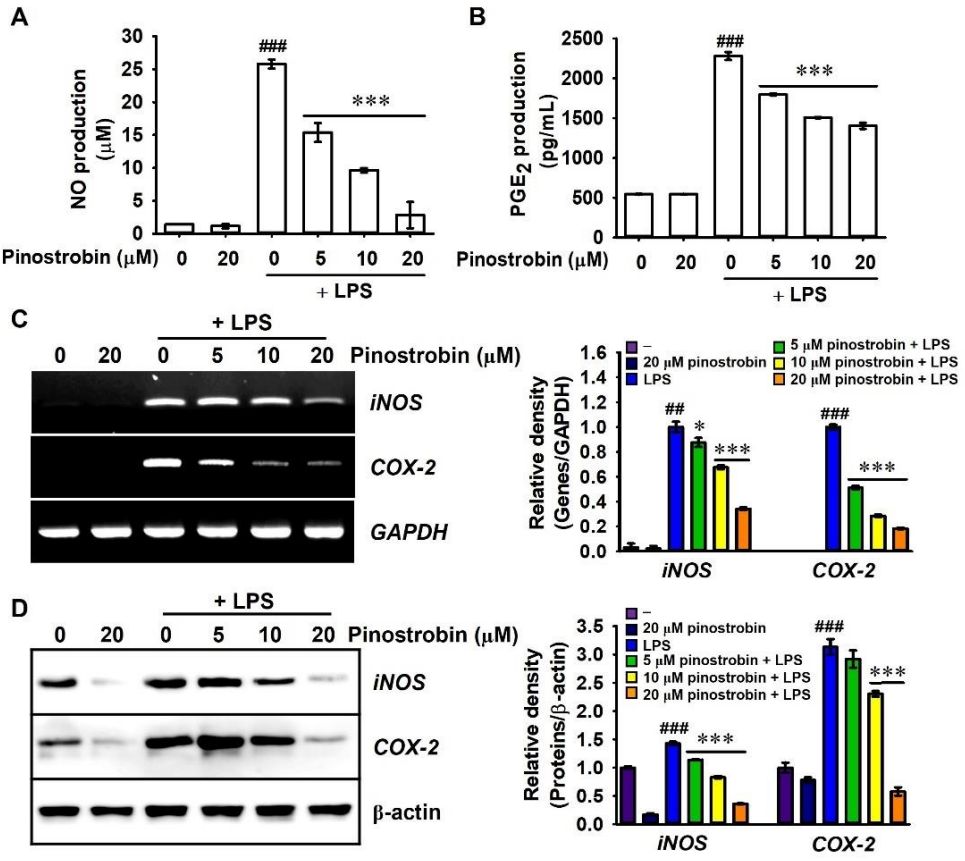

Fig. **1.** Pinostrobin suppresses LPS-stimulated NO and PGE_2 production along with iNOS and COX-2 expression. RAW264.7 macrophages were pretreated with the indicated concentrations of pinostrobin (0–20 μM) for 2 h followed by treatment with 300 ng/mL LPS for 24 h. Release of (A) NO and (B) PGE_2 to the culture media was measured using Griess reagent assay and ELISA, respectively. (C) Total RNA was extracted 6 h after LPS treatment, and RT-PCR was performed. The expression of *iNOS* and *COX-2* was normalized relative to *GAPDH* expression. (D) After 12 h-incubation with LPS, cell lysates were prepared for western blotting. β-Actin was used to normalize iNOS and COX-2 expression. The relative density was calculated using ImageJ software. $^{\#\#}$, $p < 0.01$ and $^{\#\#\#}$, $p < 0.001$ vs. untreated cells; *, $p < 0.05$ and ***, $p < 0.001$ vs. LPS-treated cells.

3.3. Pinostrobin decreases LPS-induced IL-12 and TNF-α production in LPS-stimulated RAW 264.7 macrophages

Next, we examined the potential effects of pinostrobin on the production of proinflammatory cytokines, including IL-12 and TNF-α, in LPS-stimulated RAW 264.7 macrophages. As shown in Fig. 3A and Fig. 3B, IL-12 and TNF-α were weakly expressed in the untreated cells (235.5 ± 4.5 pg/mL, 101.7 ± 0.4 pg/mL, respectively); however, LPS stimulation significantly increased IL-12 (1206.0 ± 4.9 pg/mL) and TNF-α (1563.1 ± 44.9 pg/mL) release at 24 h. Pretreatment with pinostrobin prevented LPS-induced IL-12 and TNF-α release in a concentration-dependent manner, and pinostrobin at the highest concentration (20 μM) maximally attenuated the expression (879.7 ± 5.4 pg/mL IL-12 and 627.7 ± 3.2 pg/mL TNF-α). To confirm whether pinostrobin downregulated LPS-induced *IL-12* and *TNF-α* expression, we performed RT-PCR analysis 6 h after LPS treatment. In LPS-stimulated RAW 264.7 macrophages, RT-PCR data showed that pinostrobin reduced *IL-12* and *TNF-α* expression in a concentration-dependent manner (Fig. 3C). These data indicated that pinostrobin downregulates LPS-stimulated IL-12 and TNF-α release by inhibiting gene expression.

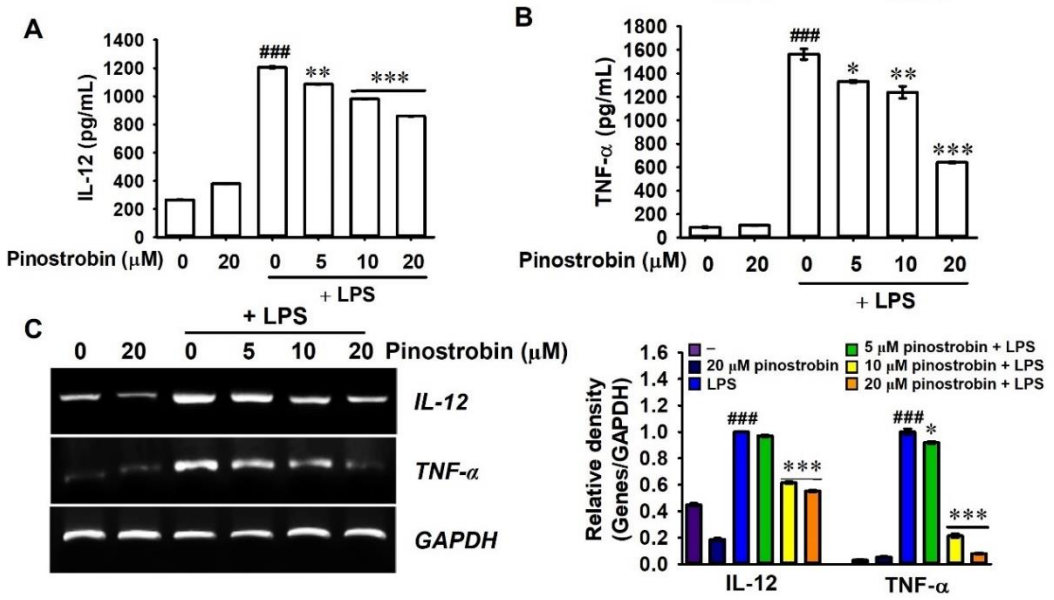

Fig. 3. Pinostrobin downregulates LPS-stimulated IL-12 and TNF-α production by suppressing their gene expression. RAW 264.7 macrophages were pretreated with pinostrobin (0–20 μM) 2 h before incubation with 300 ng/mL LPS. After 24-h incubation with LPS, (A) IL-12 and (B) TNF-α release was measured in the culture supernatants using ELISA. (C) Total RNA was extracted 6 h after LPS treatment, and RT-PCR was performed. *GAPDH* was used for normalizing *IL-12* and *TNF-α* expression. The relative density was calculated using ImageJ software. $^{###}$, $p < 0.001$ vs. untreated cells; *, $p < 0.05$, **, $p < 0.001$, and ***, $p < 0.001$ vs. LPS-treated cells.

3.4. Pinostrobin downregulates nuclear translocation of NF-κB in LPS-stimulated RAW 264.7 macrophages

As NF-κB is a key transcription factor that regulates the expression of proinflammatory mediators and cytokines [13, 14], we investigated whether pinostrobin downregulates the nuclear translocation of NF-κB in LPS-treated RAW 264.7 macrophages. As shown in Fig. 4A, LPS remarkably increased the expression of p50 and p65 in the nucleus; however, pinostrobin downregulated their expression. In addition, as shown in immunostaining of p65 in LPS-treated RAW 264.7 macrophages, pinostrobin inhibited LPS-induced nuclear translocation of p65 (Fig. 4B). These data suggest that pinostrobin inhibits the expression of proinflammatory mediators and cytokines by suppressing the nuclear translocation of NF-κB.

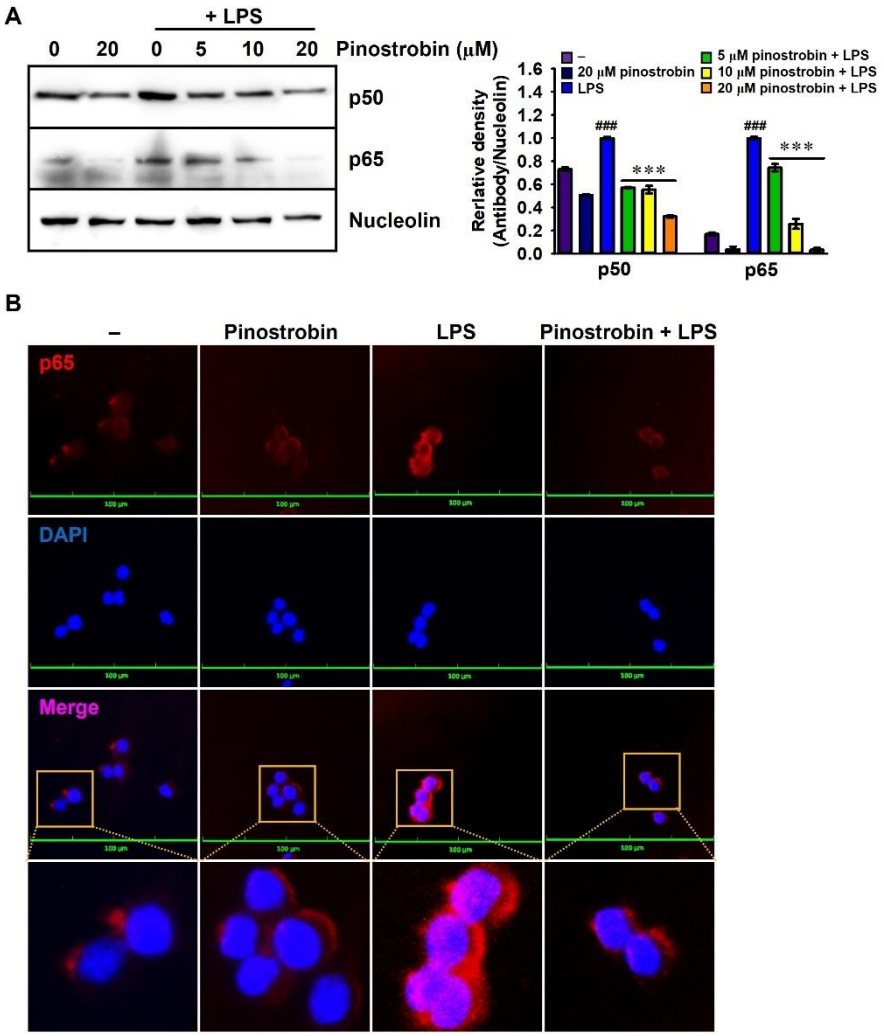

Fig. 4. Pinostrobin downregulates nuclear accumulation of NF-κB. (A) RAW 264.7 macrophages were pretreated with pinostrobin (0–20 μM) 2 h before treatment with 300 ng/mL LPS for 30 min. nuclear proteins were collected and used for western blotting. Nucleolin was used for normalizing p50 and p65 expression. The relative density was calculated using ImageJ software. (B) In a parallel experiment, p65 was immunostained with anti-p65 antibody (Ab) and detected using secondary Ab conjugated with Alexa Fluor 647 (red) followed by DAPI (blue) staining for nuclei. The fluorescence was analyzed using CELENA S digital imaging system. $^{###}$, $p < 0.001$ vs. untreated cells; ***, $p < 0.001$ vs. LPS-treated cells.

3.5. Pinostrobin potently binds to the TLR4/MD2 complex

LPS binding to the TLR4/MD2 complex on the membrane stimulates the NF-κB signaling pathway, resulting in high expression of proinflammatory genes, including *iNOS*, *COX-2*, *IL-12*, and *TNF-α* [29]. Therefore, we evaluated the potential binding of pinostrobin to the TLR4/MD2 complex. Molecular docking revealed four binding positions by which pinostrobin binds to the TLR4/MD2 complex. The strongest binding activity (pose 1) did not form hydrogen bonds but had a binding score of -5.5 (Fig. 5A and Table 3). In pose 1, pinostrobin occluded binding by interfering with the hydrophobic pocket of MD2, where LPS binds. At the same time, a hydrogen bond was formed between ARG90 of MD2 and GLU439 of TLR4, indicating that pinostrobin induces a rare interaction between MD2 and TLR4 (Fig. 5A, right). Furthermore, the 2D interaction diagram revealed that pinostrobin forms a specific carbon hydrogen bond with LYS89 in MD2, and π-alkyl or alkyl and van der Waals interactions with the TLR4/MD2 complex (Fig. 5B). In pose 2, pinostrobin formed a hydrogen bond at a distance of 2.902 Å with SER483 of TLR4, and the docking score was -4.9 (Fig. 6 and Table 3). The 2D interaction diagram showed that pinostrobin forms hydrogen bonds with GLN436 and SER438 of TLR4, and π-alkyl or alky interactions (PRO88 in MD2, and ARG460 and ALA462 in TLR4) in pose 2 (Fig. 7). In pose 3, pinostrobin showed -4.8 docking score (Table 3), but no clear hydrogen bonding was observed, and only two π-alkyl or alkyl interactions (PRO88 in MD2 and ARG460 in TLR4) were confirmed (Fig. 7). In pose 4, pinostrobin formed two hydrogen bonds with SER438 and AGR460 of TLR4 at distances of 3.076 Å and 1.947 Å, respectively (Fig. 6 and Table 3). The 2D interaction diagram in pose 4 revealed a hydrogen bond with ARG460 of TLR4, and π-alkyl or alkyl interactions with PRO88 in MD2 and ALA462 in TLR4 (Fig. 7). These data indicated that pinostrobin fits into the LPS-binding site between

LPS and the TLR4/MD2 complex and interferes with the binding of LPS to the TLR4/MD2 complex.

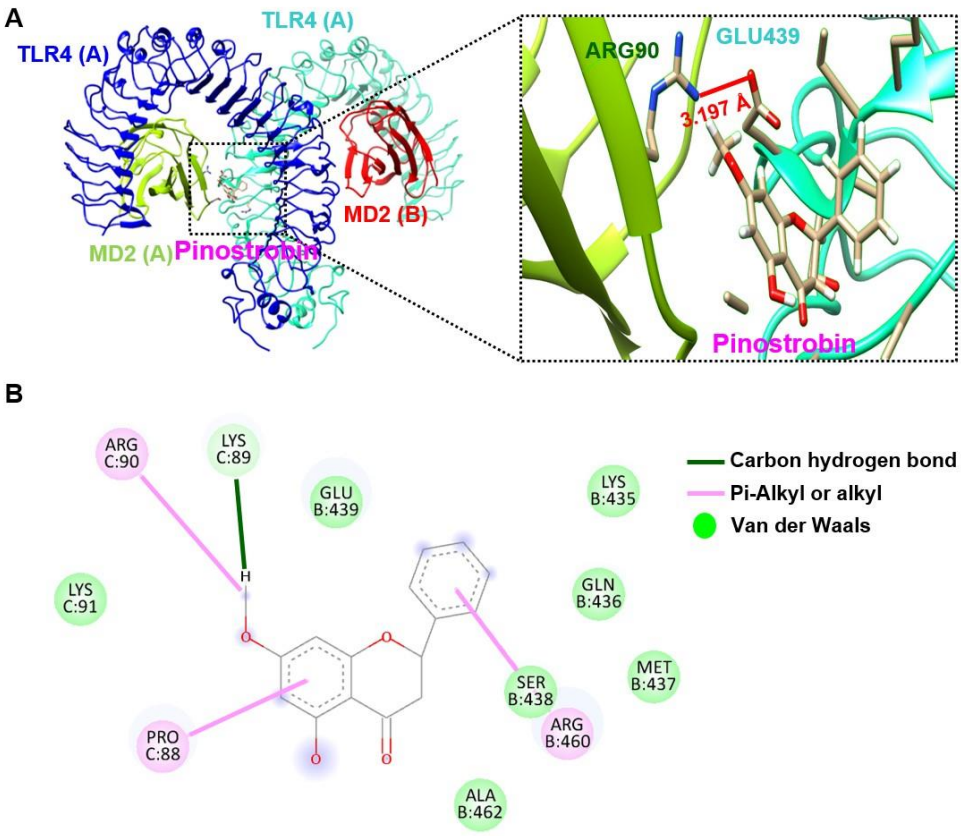

Fig. 5. Pinostrobin possibly binds to the TLR4/MD2 complex. (A) The ribbon model (pose 1, the strongest binding pose) represents that pinostrobin fits into the TLR4/MD2 complex (PDB; 3FXI, left). MD2 (red and chartreuse) and TLR4 (cyan and blue) are shown. Block dotted square shows the binding site and enlarged (right). (B) 2D interaction diagram from pose 1 was obtained using BIOVIA Discovery Studio Visualizer. Green line, carbon hydrogen bond; pink line, π-alkyl, or alky interactions; light green circle, van der Waals interactions.

Table 3. Docking poses, scores, hydrogen bond interactions, hydrogen bond distances of pinostrobin with the TLR4/MD2 complex (PDB ID: 3FXI).

Receptor	Docking pose	Docking score	Binding A.A. (H-bond)	H-bond distance (Å)
TLR4/MD2 (3FXI)	1	-5.5	-	-
	2	-4.9	SER438 (B OG)	2.902
	3	-4.8	-	-
			SER438 (B OG)	3.076
	4	-4.6	AGR460 (B O)	1.947

A.A., amino acid; H-bond; hydrogen bond.

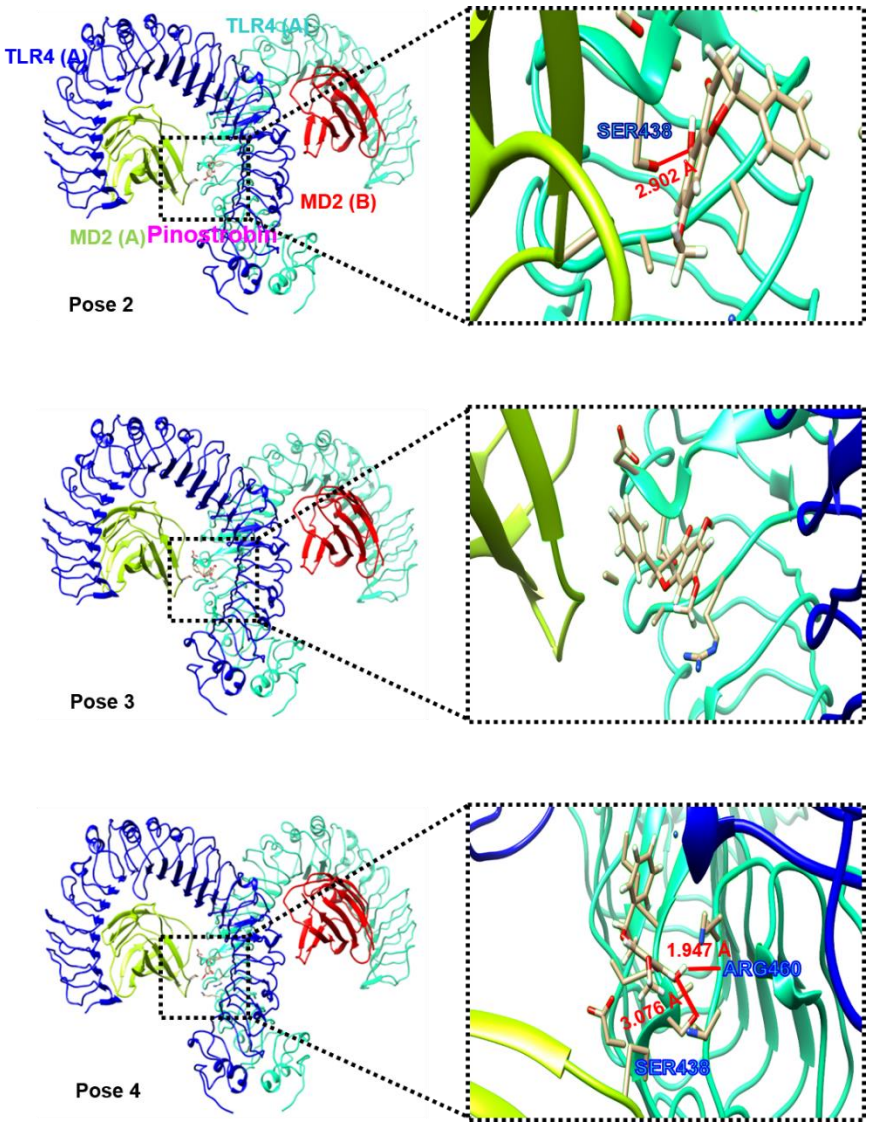

Fig. 6. Pinostrobin possibly binds to the TLR4/MD2 complex. (A) The ribbon model (from top, pose 2, pose 3, and pose 4) represents that pinostrobin fits into the TLR4/MD2 complex (PDB; 3FXI, left). MD2 (red and chartreuse) and TLR4 (cyan and blue) are shown. Block dotted square shows the binding site and enlarged (right).

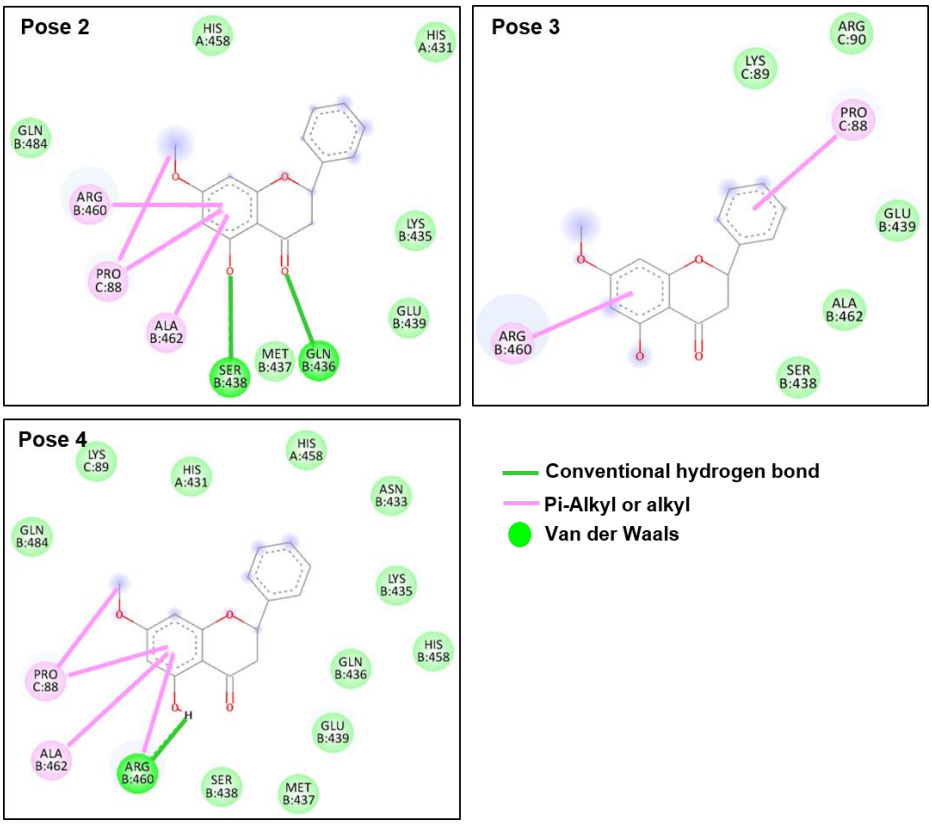

Fig. 7. Pinostrobin possibly binds to the TLR4/MD2 complex. 2D interaction diagram from pose 2~4 (clockwise) was obtained using BIOVIA Discovery Studio Visualizer. Green line, carbon hydrogen bond; pink line, π-alkyl or alky interactions; light green circle, van der Waals interactions.

3.6. Pinostrobin decreases mortality and abnormalities in LPS-microinjected zebrafish larvae

To evaluate the anti-endotoxemia effect of pinostrobin, zebrafish larvae at 3 dpf were microinjected with LPS in the presence or absence of pinostrobin, and mortality, heart rate, and abnormalities were monitored. After 24 h (at 4 dpf), LPS microinjection resulted in a significant decrease of the heart rate (144.8 ± 0.9 heartbeat/min) compared to that in PBS-microinjected larvae (179.6 ± 2.3 heartbeats/min, Fig. 8A). Upon increasing the concentrations of pinostrobin, the impaired heart rate gradually recovered almost up to the normal level at 20 μM (174.8 ± 1.9 heart beats/min). After 48 h (at 5 dpf), LPS microinjection induced a 40% death rate and 50% abnormalities in zebrafish larvae, and 10% of zebrafish larvae survived (Table 4). In contrast, pinostrobin gradually decreased the death rate and abnormalities in LPS-microinjected zebrafish larvae (Table 4). Pinostrobin at a concentration of 5 μM reduced the death rate by 10%, whereas the abnormality slightly increased to 60%. Meanwhile, 10 μM or more pinostrobin completely blocked LPS microinjection-induced death rate and strongly inhibited abnormalities (30% and 10% at 10 and 20 μM, respectively). In particular, LPS-microinjected zebrafish showed abnormalities at 5 dpf showed 50% abnormalities (Fig. 8B), displaying cyrtosis (5%), yolk necrosis (5%), yolk sac edema (5%), yolk crenulation (10%), swollen pericardium sac (15%), and head malformations (5%, Fig. 8C, left). Zebrafish larvae treated with 20 μM pinostrobin strongly blocked the abnormalities induced by LPS microinjection, and only 5% cyrtosis and 5% pericardial edema were observed (Fig. 8C, right). These data indicated that pinostrobin attenuated LPS-induced endotoxemia in zebrafish larvae.

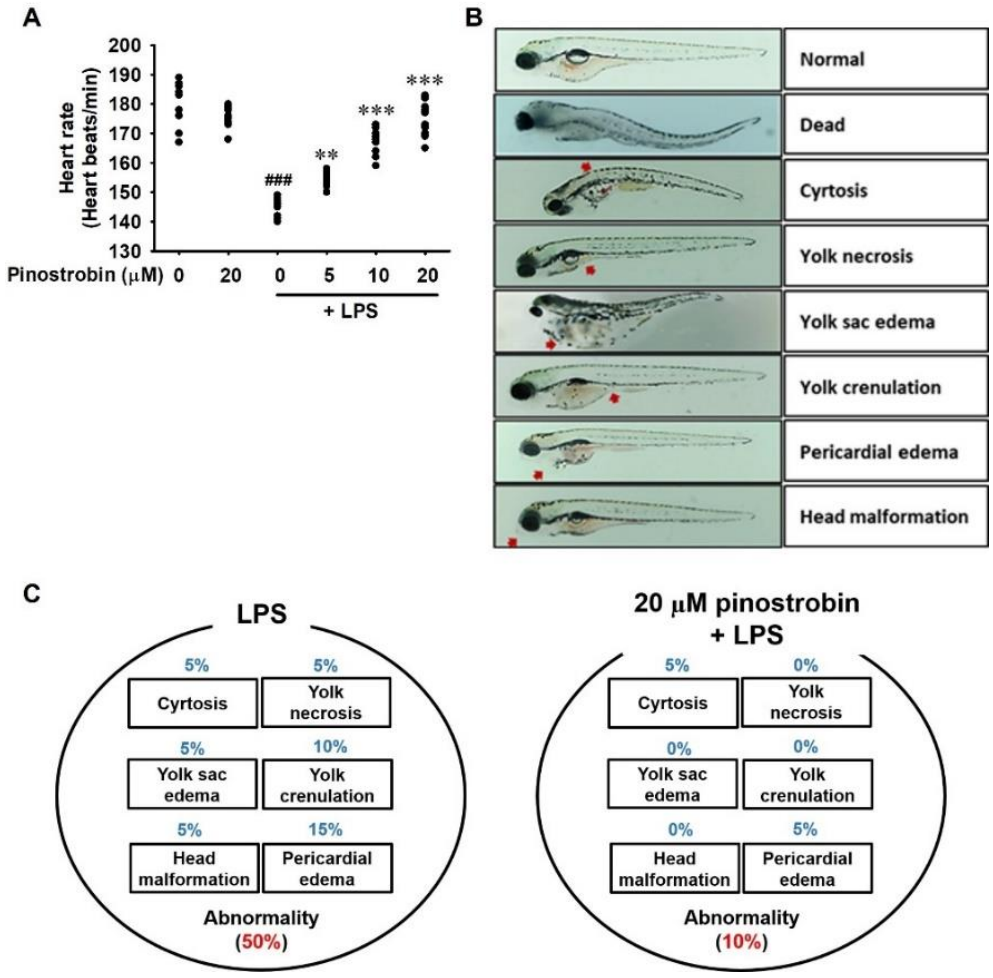

Fig. 8. Pinostrobin recovers heart rate and attenuates mortality and abnormality in LPS microinjected zebrafish larvae. Zebrafish larvae at 3 dpf (*n=20*) were microinjected with 2 nL of 0.5 mg/mL LPS and immediately treated with the indicated concentrations of pinostrobin (0–20 μM). (A) After 24 h (at 4 dpf), heart rate was measured by manually counting heartbeats per minute to assess cardiotoxicity. $^{###}$, $p < 0.001$ vs. untreated zebrafish larvae; **, $p < 0.01$ and ***, $p < 0.001$ vs. LPS-microinjected zebrafish larvae. (B) Phenotype-based evaluations were performed 48 h (at 5 dpf) after LPS microinjection. LPS microinjection increases abnormalities in zebrafish larvae; normal, death, cyrtosis, yolk necrosis, yolk sac edema yolk crenulation, pericardial edema, and head malformation. (C) LPS microinjection induced 50% abnormalities in zebrafish larvae (left), and pinostrobin (20 μM)-treated zebrafish reduced the abnormality to 10% (right).

Table 4. Effects of pinostrobin on mortality and abnormality in LPS-microinjected zebrafish larvae.

Group	Phenotype (%)/48 h (*n=20*)		
	Normal	Death	Abnormality
untreated	100	0	0
20 μM pinostrobin	100	0	0
LPS	10	40	50
5 μM pinostrobin + LPS	30	10	60
10 μM pinostrobin + LPS	70	0	30
20 μM pinostrobin + LPS	90	0	10

3.7. Pinostrobin attenuates recruitment macrophages and neutrophils in LPS-microinjected zebrafish larvae accompanied by downregulation of proinflammatory genes

The effects of pinostrobin on LPS-induced macrophage and neutrophil infiltration in zebrafish larvae were further investigated by neutral red and Sudan black staining, respectively. As shown in Fig. 9A, neutral red staining showed the number of macrophages was predominately elevated in the yolk sac where LPS was microinjected compared to that in the PBS-microinjected larvae. However, pinostrobin treatment significantly reduced the accumulation of macrophages at the site of inflammation in a concentration-dependent manner. In addition, in PBS-microinjected zebrafish, a large number of neutrophils stained with Sudan black were seen in the posterior blood island (PBI), which is a hematopoietic site, but LPS microinjection into the yolk sac clearly reduced neutrophils in the PBI (Fig. 9B), indicating that neutrophils migrated from the PBI to the site of infection. However, in LPS-microinjected zebrafish larvae, pinostrobin significantly reduced neutrophil recruitment in a concentration-dependent manner. Furthermore, in LPS-microinjected larvae at 4 dpf, the expression of proinflammatory genes, including *iNOS*, *COX-2a*, *IL-12*, and *TNF-α*, was high (Fig. 9C). However, pinostrobin concentration-dependently decreased the expression of the genes in LPS-microinjected zebrafish larvae. These data indicate that pinostrobin potently inhibits endotoxemia by suppressing the recruitment of macrophages and neutrophils concomitant with downregulation of proinflammatory gene expression.

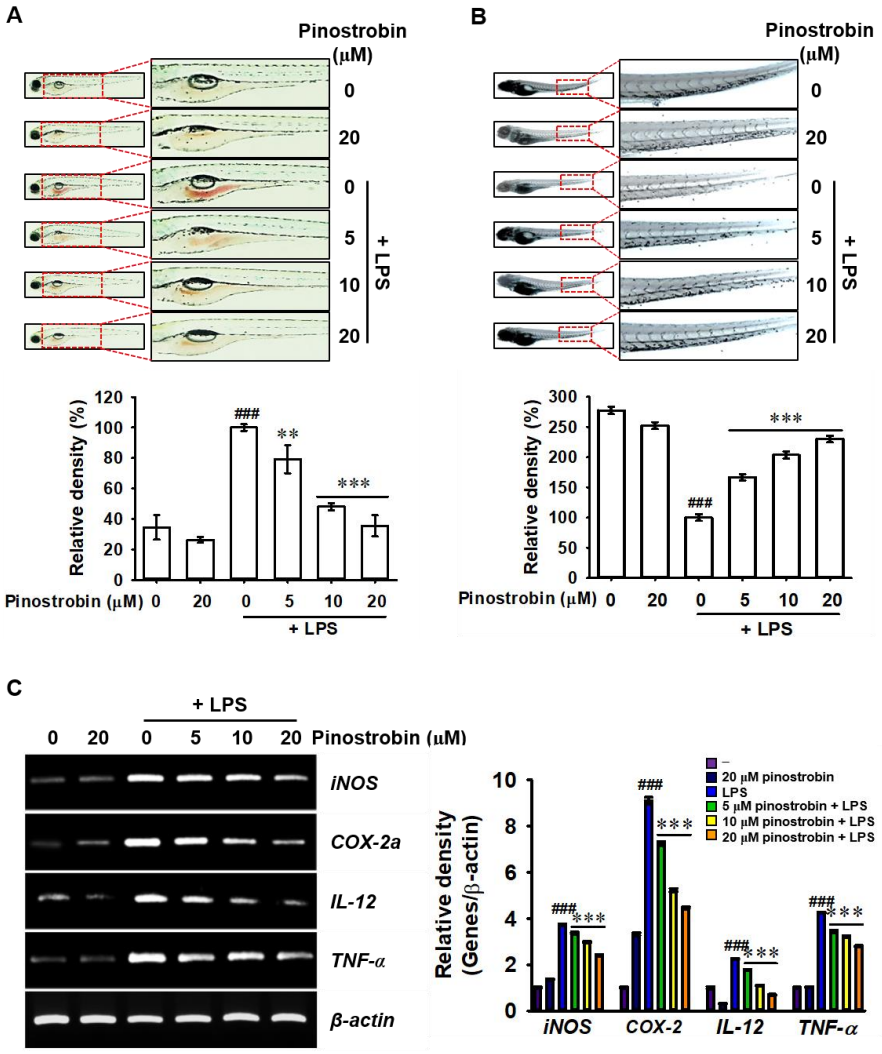

Fig. 9. Pinostrobin reduces LPS-induced macrophage and neutrophil recruitment in zebrafish larvae. Zebrafish larvae at 3 dpf (*n=20*) were microinjected with 2 nL of 0.5 mg/mL LPS and immediately treated with pinostrobin (0–20 μM) for 24 h (at 4 dpf). (A) Neutral red staining of macrophages and (B) Sudan black staining for neutrophils were performed. (C) In a parallel experiment, total RNA was isolated, and RT-PCR was performed. The expression of *iNOS*, *COX-2a*, *IL-12*, and *TNF-α* was measured and normalized compared to that of β-actin expression. $^{###}$, $p < 0.001$ vs. PBS-microinjected zebrafish larvae; **, $p < 0.01$ and ***, $p < 0.001$ vs. LPS-microinjected zebrafish larvae.

4. Discussion

Pinostrobin was first discovered in *Pinus strobus* L. and is known to possess various pharmacological properties, including anti-inflammatory, anti-viral, anti-bacterial, and anti-cancer [20]. In particular, Panthong et al. [30] demonstrated that pinostrobin inhibits carrageenan-induced paw edema in Sprague-Dawley rats by 11.5%. Patel and Bhutani [22] reported that pinostrobin attenuated LPS-stimulated TNF-α and IL-1β levels at 22–40 μM. In addition, pinostrobin inhibited NO production by 50% at approximately 43 μM [31], and COXs were weakly inhibited at a concentration of 100 μg/mL [32]. Nevertheless, the anti-inflammatory mechanism of pinostrobin is not well known. Therefore, in this study, we evaluated whether pinostrobin induces anti-inflammatory activity in LPS-stimulated RAW 264.7 macrophages and anti-endotoxemia effect in LPS-microinjected zebrafish larvae. Additionally, through molecular docking, we investigated the effect of pinostrobin on LPS-induced inflammatory signaling.

Macrophages are representative cells of the innate immune system that establish the first line of defense against invading pathogens [33]. By various stimulants such as LPS and granulocyte-macrophage colony-stimulating factor, native macrophages are polarized to proinflammatory macrophages (M1), and the expression of various proinflammatory mediators, NO and PGE_2, and cytokines, IL-12 and TNF-α, is increased, which rapidly eliminates pathogens and strengthens primary host defense and tissue integrity [34, 35]. However, overactivated M1 macrophages stimulate persistent proinflammatory mediators and cytokines and collapse the balance of the immune response, causing tissue damage [36]. LPS binds to the TLR4/MD2 complex and overactivates intracellular signaling, thereby causing endotoxemia [37]. In addition, macrophages and neutrophils migrate toward the inflammatory site,

accompanied by upregulation of inflammatory cytokines, including IL-12 and TNF-α [38]. Niwano et al. [39] reported that many polyphenols might be safe and promising therapeutics for the prevention and treatment of LPS-induced inflammatory disorders. In this study, we determined that pinostrobin attenuated LPS-stimulated inflammation and endotoxemia in zebrafish larvae accompanied by a significant decrease in proinflammatory genes. Pinostrobin strongly inhibited LPS microinjection-induced mortality and abnormalities by suppressing the recruitment of macrophages and neutrophils. These results show that pinostrobin is a promising candidate for the control of LPS-induced hyperinflammatory responses, such as endotoxemia.

LPS binding to the TLR4/MD2 complex triggers two intracellular signaling pathway; one initiates the recruitment of the intracellular adaptor molecule MyD88, which subsequently stimulates the NF-κB-mediated inflammatory response, and the other begins to bind TRIF to the intracellular domain of the endosome through CD14-mediated endocytosis, which initiates anti-viral activity [29]. The MyD88-dependent signaling pathway subsequently induces the activation of IKK and IRAKs and triggers inflammatory responses through the activation of NF-κB [11, 12]. NF-κB is mainly composed of two protein subunits, p50 and p65, and exists in the cytosol in its inactive form by binding to the inhibitory protein of IκB [14, 40]. When exposed to proinflammatory stimuli, such as LPS, IKK is rapidly phosphorylated and IκB releases NF-κB subunits, such as p50 and p65, which are translocated to the nucleus and consequently transactivate proinflammatory genes, including *iNOS*, *COX-2*, *IL-12*, and *TNF-α*. Therefore, many natural antagonists targeting TLR4 have been developed and applied in clinical trials [41]. In this study, we found that pinostrobin potently fits into the TLR4/MD2 complex, which hinders the normal binding between TLR4 and MD2. Resman et al. [42] showed that, for endotoxin transfer from CD14 to MD2, VAL82,

MET85, and LEU87, which are hydrophobic pockets of MD2, are essential; these sites also play an important role in binding to TLR4. In addition, hydrophobic residues, PHE440 and PHE436, located in leucine-rich repeats 16 and 17 of TLR4, are inevitable amino acid residues for TLR4 activation by LPS [42]. According to our data, pinostrobin forms carbon hydrogen bonds with LYS89 of MD2, and π-alkyl or alkyl interactions with PRO88 and ARG90 of MD2 in pose 1. Moreover, pinostrobin forms van der Waals interactions with LYS435-GLN436-MET437-SER438-GLU439, a key hydrophobic residue for TLR4 binding to LPS. These results indicate that pinostrobin occludes the hydrophobic pockets of MD2 and TLR4 and blocks LPS binding, thereby exhibiting an anti-inflammatory activity.

In summary, our results demonstrate that pinostrobin exerts anti-inflammatory effects in LPS-stimulated RAW 264.7 macrophages. Moreover, pinostrobin noticeably attenuated the mortality and abnormalities in LPS-microinjected zebrafish larvae. The anti-inflammatory and anti-endotoxemia effects occur because pinostrobin binds to the TLR4/MD2 complex and inhibits the intracellular signaling process, leading to NF-κB activation. Finally, we conclude that pinostrobin may be a potential candidate for use as an anti-inflammatory agent.

References

[1] D. Li, M. Wu, Pattern recognition receptors in health and diseases, Signal Transduct. Target. Ther. 6(1) (2021) 291.

[2] C. Shi, E.G. Pamer, Monocyte recruitment during infection and inflammation, Nat. Rev. Immunol. 11(11) (2011) 762-774.

[3] L.A. Abdulkhaleq, M.A. Assi, R. Abdullah, M. Zamri-Saad, Y.H. Taufiq-Yap, M.N.M. Hezmee, The crucial roles of inflammatory mediators in inflammation: A review, Vet. World 11(5) (2018) 627-635.

[4] G. Schett, M.F. Neurath, Resolution of chronic inflammatory disease: Universal and tissue-specific concepts, Nat. Commun. 9(1) (2018) 3261.

[5] J.M. Bennett, G. Reeves, G.E. Billman, J.P. Sturmberg, Inflammation-nature's way to efficiently respond to all types of challenges: Implications for understanding and managing "the epidemic" of chronic diseases, Front. Med. (Lausanne) 5 (2018) 316.

[6] S. Chakraborty, S.D. Zawieja, W. Wang, Y. Lee, Y.J. Wang, P.Y. von der Weid, D.C. Zawieja, M. Muthuchamy, Lipopolysaccharide modulates neutrophil recruitment and macrophage polarization on lymphatic vessels and impairs lymphatic function in rat mesentery, Am. J. Physiol. Heart Circ. Physiol. 309(12) (2015) H2042-H2057.

[7] K. Dhaliwal, E. Scholefield, D. Ferenbach, M. Gibbons, R. Duffin, D.A. Dorward, A.C. Morris, D. Humphries, A. MacKinnon, T.S. Wilkinson, W.A. Wallace, N. van Rooijen, M. Mack, A.G. Rossi, D.J. Davidson, N. Hirani, J. Hughes, C. Haslett, A.J. Simpson, Monocytes control second-phase neutrophil emigration in established lipopolysaccharide-induced murine lung injury, Am. J. Respir. Crit. Care Med. 186(6) (2012) 514-524.

[8] S.J. Kim, H.M. Kim, Dynamic lipopolysaccharide transfer cascade to TLR4/MD2 complex via LBP and CD14, BMB Rep. 50(2) (2017) 55-57.

[9] J.K. Ryu, S.J. Kim, S.H. Rah, J.I. Kang, H.E. Jung, D. Lee, H.K. Lee, J.O. Lee, B.S. Park, T.Y. Yoon, H.M. Kim, Reconstruction of LPS transfer cascade reveals structural determinants within LBP, CD14, and TLR4-MD2 for efficient LPS recognition and transfer, Immunity 46(1) (2017) 38-50.

[10] E. Guven-Maiorov, O. Keskin, A. Gursoy, C. VanWaes, Z. Chen, C.J. Tsai, R. Nussinov, The architecture of the TIR domain signalosome in the Toll-like receptor-4 signaling pathway, Sci. Rep. 5 (2015) 13128.

[11] R. Deliz-Aguirre, F. Cao, F.H.U. Gerpott, N. Auevechanichkul, M. Chupanova, Y. Mun, E. Ziska, M.J. Taylor, MyD88 oligomer size functions as a physical threshold to trigger IL1R Myddosome signaling, J. Cell. Biol. 220(7) (2021) e202012071.

[12] K.R. Balka, D. De Nardo, Understanding early TLR signaling through the Myddosome, J. Leukoc. Biol. 105(2) (2019) 339-351.

[13] J.P. Mitchell, R.J. Carmody, NF-κB and the transcriptional control of inflammation, Int. Rev Cell Mol. Biol. 335 (2018) 41-84.

[14] T. Liu, L. Zhang, D. Joo, S.C. Sun, NF-κB signaling in inflammation, Signal Transduct. Target. Ther. 2 (2017) 17023.

[15] M.A. Anwar, M. Shah, J. Kim, S. Choi, Recent clinical trends in Toll-like receptor targeting therapeutics, Med. Res. Rev. 39(3) (2019) 1053-1090.

[16] A.N. Panche, A.D. Diwan, S.R. Chandra, Flavonoids: An overview, J. Nutr. Sci. 5 (2016) e47.

[17] X. He, H. Zhang, X. Liang, Separation of six compounds from pigeon pea leaves by elution-extrusion counter-current chromatography, J. Sep. Sci. 42(6) (2019)

1202-1209.

[18] S.I. Abdelwahab, S. Mohan, M.A. Abdulla, M.A. Sukari, A.B. Abdul, M.M. Taha, S. Syam, S. Ahmad, K.H. Lee, The methanolic extract of *Boesenbergia rotunda* (L.) Mansf. and its major compound pinostrobin induces anti-ulcerogenic property in vivo: Possible involvement of indirect antioxidant action, J. Ethnopharmacol. 137(2) (2011) 963-970.

[19] H.A. Jung, A.R. Kim, H.Y. Chung, J.S. Choi, In vitro antioxidant activity of some selected Prunus species in Korea, Arch. Pharm. Res. 25(6) (2002) 865-872.

[20] N.K. Patel, G. Jaiswal, K.K. Bhutani, A review on biological sources, chemistry and pharmacological activities of pinostrobin, Nat. Prod. Res. 30(18) (2016) 2017-2027.

[21] L. Poblocka-Olech, I. Inkielewicz-Stepniak, M. Krauze-Baranowska, Anti-inflammatory and antioxidative effects of the buds from different species of Populus in human gingival fibroblast cells: Role of bioflavanones, Phytomedicine 56 (2019) 1-9.

[22] N.K. Patel, K.K. Bhutani, Pinostrobin and Cajanus lactone isolated from *Cajanus cajan* (L.) leaves inhibits TNF-α and IL-1β production: In vitro and in vivo experimentation, Phytomedicine 21(7) (2014) 946-953.

[23] W. Karunarathne, I.M.N. Molagoda, K.T. Lee, Y.H. Choi, C.Y. Jin, G.Y. Kim, Anthocyanin-enriched polyphenols from *Hibiscus syriacus* L. (Malvaceae) exert anti-osteoporosis effects by inhibiting GSK-3β and subsequently activating β-catenin, Phytomedicine 91 (2021) 153721.

[24] R. Kiss, F. Szalai, M. Sandor, Mcule.com: A public web service for drug discovery, Abstr. Pap. Am. Chem. S 243 (2012).

[25] E.F. Pettersen, T.D. Goddard, C.C. Huang, G.S. Couch, D.M. Greenblatt, E.C.

Meng, T.E. Ferrin, UCSF Chimera--a visualization system for exploratory research and analysis, J. Comput. Chem. 25(13) (2004) 1605-1612.

[26] C.B. Kimmel, W.W. Ballard, S.R. Kimmel, B. Ullmann, T.F. Schilling, Stages of embryonic development of the zebrafish, Dev. Dyn. 203(3) (1995) 253-310.

[27] B.A. Weeks, A.S. Keisler, Q.N. Myrvik, J.E. Warinner, Differential uptake of neutral red by macrophages from three species of estuarine fish, Dev. Comp. Immunol. 11(1) (1987) 117-124.

[28] K.B. Walters, J.M. Green, J.C. Surfus, S.K. Yoo, A. Huttenlocher, Live imaging of neutrophil motility in a zebrafish model of WHIM syndrome, Blood 116(15) (2010) 2803-2811.

[29] A. Ciesielska, M. Matyjek, K. Kwiatkowska, TLR4 and CD14 trafficking and its influence on LPS-induced pro-inflammatory signaling, Cell. Mol. Life Sci. 78(4) (2021) 1233-1261.

[30] A. Panthong, D. Kanjanapothi, P. Tuntiwachwuttikul, O. Pancharoen, V. Reutrakul, Antiinflammatory activity of flavonoids, Phytomedicine 1(2) (1994) 141-144.

[31] C. Lee, J.W. Lee, Q. Jin, D.S. Jang, S.J. Lee, D. Lee, J.T. Hong, Y. Kim, M.K. Lee, B.Y. Hwang, Inhibitory constituents of the heartwood of *Dalbergia odorifera* on nitric oxide production in RAW 264.7 macrophages, Bioorg. Med. Chem. Lett. 23(14) (2013) 4263-4266.

[32] D. Wu, M.G. Nair, D.L. DeWitt, Novel compounds from *Piper methysticum* Forst (Kava Kava) roots and their effect on cyclooxygenase enzyme, J. Agric. Food Chem. 50(4) (2002) 701-705.

[33] J.L. Mege, V. Mehraj, C. Capo, Macrophage polarization and bacterial infections, Curr. Opin. Infect. Dis. 24(3) (2011) 230-234.

[34] C.D. Mills, K. Ley, M1 and M2 macrophages: The chicken and the egg of immunity, J. Innate Immun. 6(6) (2014) 716-726.

[35] L. Peng, R. van den Biggelaar, C.A. Jansen, H.P. Haagsman, E.J.A. Veldhuizen, A method to differentiate chicken monocytes into macrophages with proinflammatory properties, Immunobiology 225(6) (2020) 152004.

[36] D.L. Laskin, V.R. Sunil, C.R. Gardner, J.D. Laskin, Macrophages and tissue injury: agents of defense or destruction?, Annu. Rev. Pharmacol. Toxicol. 51 (2011) 267-288.

[37] F.F. Anhe, N.G. Barra, J.F. Cavallari, B.D. Henriksbo, J.D. Schertzer, Metabolic endotoxemia is dictated by the type of lipopolysaccharide, Cell Rep. 36(11) (2021) 109691.

[38] D.R. Powell, A. Huttenlocher, Neutrophils in the tumor microenvironment, Trends Immunol. 37(1) (2016) 41-52.

[39] Y. Niwano, H. Kohzaki, M. Shirato, S. Shishido, K. Nakamura, Putative mechanisms underlying the beneficial effects of polyphenols in murine models of metabolic disorders in relation to gut microbiota, Curr. Issues Mol. Biol. 44(3) (2022) 1353-1375.

[40] T. Liu, L. Zhang, D. Joo, S.-C. Sun, NF-κB signaling in inflammation, Signal Transduct. Target. Ther. 2 (2017) 17023.

[41] J.S.Y. Tam, J.K. Coller, P.A. Hughes, C.A. Prestidge, J.M. Bowen, Toll-like receptor 4 (TLR4) antagonists as potential therapeutics for intestinal inflammation, Indian J. Gastroenterol. 40(1) (2021) 5-21.

[42] N. Resman, J. Vasl, A. Oblak, P. Pristovsek, T.L. Gioannini, J.P. Weiss, R. Jerala, Essential roles of hydrophobic residues in both MD-2 and toll-like receptor 4 in activation by endotoxin, J. Biol. Chem. 284(22) (2009) 15052-15060.

PART 02

Pinostrobin suppresses tyrosinase activity and α-MSH-induced melanogenic signaling pathway

Abstract

Pinostrobin is a dietary flavonoid found in several plants that possesses pharmacological properties, such as anti-cancer, anti-virus, antioxidant, anti-ulcer, and anti-aromatase effects. However, it is unclear whether pinostrobin exerts anti-melanogenic properties and, if so, what the underlying molecular mechanisms comprise. Therefore, in this study, we investigated whether pinostrobin inhibits melanin biosynthesis in vitro and in vivo, as well as the potential associated mechanism. Pinostrobin reduced mushroom tyrosinase activity in vitro in a concentration-dependent manner, with an IC50 of 527.7 μM. Molecular docking simulations further revealed that pinostrobin forms a hydrogen bond, as well as other non-covalent interactions, between the C-type lectin-like fold and polyphenol oxidase chain, rather than the previously known copper-containing catalytic center. Additionally, pinostrobin significantly decreased α-melanocyte-stimulating hormone (α-MSH)-induced extracellular and intracellular melanin production, and tyrosinase activity in B16F10 melanoma cells. More specifically, pinostrobin inhibited the α-MSH-induced melanin biosynthesis signaling pathway by suppressing the cAMP-CREB-MITF axis. In fact, pinostrobin also attenuated pigmentation in α-MSH-stimulated zebrafish larvae without causing cardiotoxicity. Collectively, these results indicate that pinostrobin effectively inhibits melanogenesis in vitro and in vivo via regulation of the cAMP-CREB-MITF axis.

*Key words***:** Pinostrobin; Melanogenesis; Tyrosinase; α-MSH

1. Introduction

Melanocytes are melanin-synthesizing neural crest-derived cells that exist in the basal layer of the skin [1]. Once melanin is synthesized in melanocytes, it is incorporated into the melanosome, an organelle that is transported to adjacent keratinocytes, resulting in melanin distribution [2]. Melanin, in particular, eumelanin, protects human skin from ultraviolet radiation (UVR)-induced DNA and skin damage by absorbing UVR and scavenging UVR-induced reactive oxygen species (ROS) [3]. Hence, melanin is thought to serve as the primary photoprotective pigment that suppresses UVR-induced oxidative stress and damage. However, in contrast to eumelanin, pheomelanin is photodegraded by UVR and simultaneously promotes ROS generation, leading to melanocyte and keratinocyte apoptosis [4]. Meanwhile, the unusual accumulation of melanin also causes dermatological disorders, including melasma, wrinkling, senile lentigines, and skin cancers [5, 6]. Hence, in response to the increased interest in skin whitening within the beauty industry, identification and characterization of anti-melanogenic compounds has attracted considerable attention [7, 8].

Melanogenesis is a physiological process that promotes melanin biosynthesis through enzymatic and non-enzymatic reactions. In the enzymatic pathway, tyrosinase plays an important role in increasing melanin biosynthesis through hydroxylation of tyrosine into dihydroxyphenylalanine (DOPA), followed by further oxidation into dopaquinone, which is the precursor for pheomelanin and eumelanin via cysteinyl-DOPA and dopachrome, respectively [11]. Given that tyrosinase has been recognized as a major target molecule for the inhibition of melanin biosynthesis, many antagonists have been developed and applied clinically [3]. Tyrosinase is a di-copper oxidase in which six histidine residues surround two copper ions, CuA and CuB, in its catalytically

active site [9]. Based on molecular docking data, Goldfeder et al. [10] reported that the main substrates of tyrosinase, namely, tyrosine, p-tyrosol, and L-DOPA fit in the active site, whereas the presence of Zn^{2+} ions forces out the Cu^{2+} ions, effectively inhibiting the catalytic activity. In this way, many flavonoids competitively target the active site of tyrosinase, thereby inhibiting its activity [11, 12]. Accordingly, competitive inhibitors targeting tyrosinase may represent an excellent strategy for inhibiting melanin biosynthesis.

UVR increases the expression of α-melanocyte-stimulating hormone (α-MSH) in keratinocytes, which binds to the melanocortin 1 receptor (MC1R) in melanocytes and activates a complex series of cellular signal transduction pathways that promote melanin biosynthesis [13]. Binding of α-MSH to MC1R primarily activates adenylyl cyclase (AC) in melanocytes, which increases intracellular cyclic 3',5'-cyclic adenosine monophosphate (cAMP) levels and consequently stimulates protein kinase A (PKA) [14]. Subsequently, cAMP-responsive element-binding protein (CREB) is phosphorylated, which, together with CBP/p300, promotes the expression of microphthalmia-related transcription factor (MITF), a main regulator of tyrosinase expression [15]. Therefore, considering that α-MSH functions as the primary physiological agonist of MC1R, targeting the α-MSH-mediated signaling pathway may inhibit melanin biosynthesis by suppressing tyrosinase expression.

Pinostrobin is a natural flavonoid found in various plants, such as the leaves of *Cajanus cajan* (L.) Millsp and the rhizomes of *Boesenbergia rotunda* (L.). Pinostrobin possesses a broad spectrum of pharmacological activities, including anti-cancer [16, 17], antioxidant [18], and anti-virus properties [19]. In fact, El-Nashar et al. [20] recently reported that pinostrobin, isolated from Egyptian propolis, effectively reduces in vitro mushroom tyrosinase activity by approximately 36.8% at a concentration of

100 μM. However, there is currently a dearth of data regarding the anti-melanogenic effects of pinostrobin. Therefore, in this study, we investigated whether pinostrobin downregulates melanogenesis in B16F10 melanoma cells and zebrafish larvae by inhibiting direct inhibition and the expression of tyrosinase.

2. Materials and methods

2.1. Reagents and antibodies

Dulbecco's modified Eagle's medium (DMEM), fetal bovine serum (FBS), and an antibiotic mixture were purchased from WeLGENE (Gyeongsan, Gyeongsangbuk-do, Republic of Korea). Phenylthiourea (PTU), ascorbic acid (AA), kojic acid (KA), mushroom tyrosinase, 3-(4,5-dimethylthiazol-2-yl)-2,5-diphenyltetrazolium bromide (MTT), α-MSH, and 3-isoburyl-1-methylxanthine (IBMX) were purchased from Sigma-Aldrich (St. Louis, MO, USA). Antibodies against tyrosinase (sc-20035), MITF (sc-71588), p-CREB (sc-81486), and β-actin (sc-69879) were obtained from the Santa Cruz Biotechnology (Dallas, TX, USA). Pinostrobin (Fig. 1A) was obtained from the National Institute of Forest Science (Suwon, Gyeonggi-do, Republic of Korea). All other chemicals were purchased from Sigma-Aldrich.

2.2. In vitro mushroom tyrosinase assay

Tyrosinase inhibition was measured using mushroom tyrosinase in a cell-free system by modifying the method of Duckworth and Coleman [21]. Briefly, the reaction mixture was prepared with 130 μL of 100 mM phosphate buffer (pH 6.8), 20 μL of pinostrobin, 30 μL of 1.5 mM L-tyrosine, and 20 μL of 210 U/mL mushroom tyrosinase, incubated for 30 min at 37 ℃, and absorbance was measured at 490 nm using a microplate spectrophotometer (Thermo Fisher Scientific, Rockford, IL, USA). PTU (250 nM), AA (500 μM), and KA (25 μM) were used as positive controls. The inhibition rate (%) mushroom tyrosinase in vitro was calculated using equation (1):

$$\text{Inhibition (\%)} = [A_0 – (A_1 - A_2)/A_0] – 100 \qquad (1)$$

where A_0, A_1, and A_2 are the absorbance values of the control ([L-tyrosine + tyrosinase] – L-tyrosine), samples (L-tyrosine + samples + tyrosinase), and blank (L-tyrosine + samples), respectively. The concentration required for 50% inhibition (IC_{50}) was

calculated using GraphPad Prism 9.3.1.147 (San Diego, CA, USA).

2.3. Molecular docking

The crystal structure of tyrosinase from *Agaricus bisporus* [protein database bank (PDB) ID: 2Y9X] was obtained from the RCSB PDB, and the chemical structure of pinostrobin was obtained from PubChem (https://pubchem.ncbi.nlm.nih.gov). For protein-ligand docking, simulations were performed using SwissDock [22]. A monomer of 2Y9X [a heavy (polyphenol oxidase) and a light (lectin-like fold protein) chain] was as the full structure of 2Y9X could not be uploaded to SwissDock. Molecular docking data were visualized using the UCSD Chimera. A 2D interaction diagram was constructed using Discovery Studio Visualizer (https://www.discover.3ds.com).

2.4. Cell culture and cell viability assay

Murine B16F10 melanoma cells (ATCC, Manassas, VA, USA) were maintained in DMEM supplemented with 10% heat-inactivated FBS at 37 ℃ in a humidified atmosphere containing 5% CO_2. To analyze the effect of pinostrobin on cell viability, an MTT assay was performed. Briefly, B16F10 melanoma cells were seeded in 24-well plates at a density of 1×10^4 cells/mL for 16 h. The cells were then treated with the indicated concentrations of pinostrobin (0–200 μM) for 24, 48, and 72 h. After incubation, MTT was added to each well and the plates were incubated for 4 h at 37 ℃. The precipitate was dissolved in dimethyl sulfoxide (DMSO), and the absorbance was measured at 540 nm using a microplate spectrophotometer (Thermo Fisher Scientific). Cellular morphology was observed under a stereomicroscope (MACROTECH, Goyang, Gyeonggi-do, Republic of Korea).

2.5. Flow cytometry analysis

To estimate the total viable cell count and dead cell population, flow cytometry was performed. Briefly, B16F10 melanoma cells were plated at a density of 1×10^4 cells/mL and treated with the indicated concentrations of pinostrobin (0–200 μM) for 72 h. Hydrogen peroxide (H_2O_2, 100 μM) was added for 24 h and used as a cell death-inducing control. Briefly, the cells were harvested and washed with ice-cold phosphate-buffered saline (PBS). The cells were then incubated with a Muse Cell Count & Viability Kit (Luminex, Austin, Texas, USA) for 5 min and analyzed using a Muse Cell Analyzer (Luminex).

2.6. Measurement of extracellular and intracellular melanin content

The effect of pinostrobin on α-MSH-induced melanogenesis was measured according to a previous method [28]. Briefly, B16F10 melanoma cells were cultured at 1×10^4 cell/mL in 6-well plates for 16 h and treated with α-MSH (500 ng/mL) for 24 h, followed by treatment with the indicated concentrations of pinostrobin (0–50 μM) for 48 h. Extracellular melanin content was measured using culture media at 405 nm. To measure the intracellular melanin content, the cells were washed in ice-cold PBS and dissolved in 1 N NaOH containing 10% DMSO at 100 ℃ for 10 min. The dissolved melanin content was measured at 405 nm.

2.7. Measurement of intracellular tyrosinase activity

Intracellular tyrosinase activity was measured as previously described [23]. Briefly, B16F10 melanoma cells (5×10^4 cells/mL) were pretreated with 500 ng/mL α-MSH for 24 h and the indicated concentrations of pinostrobin (0–50 μM) were incubated for 48 h. The cells were then lysed with PBS containing 1% Triton X-100 by freezing at -20 ℃ for 2 h and disrupted by thawing at room temperature. Total protein was quantified using Bio-Rad Protein Assay Reagents (Bio-Rad) and an equal amount

of protein was mixed with 90 μL of 5 mM L-DOPA at 37 ℃ for 30 min. Absorbance was measured at a wavelength of 405 nm.

2.8. Enzyme-linked immunosorbent assay (ELISA) for cAMP

B16F10 melanoma cells (5×10^4 cells/mL) were cultured in serum-free DMEM media and pretreated with 1 mM IBMX for 10 min. Pinostrobin (0–50 μM) was then added in the presence or absence of 500 ng/mL α-MSH for 15 min. Intracellular cAMP levels were measured using a colorimetric ELISA kit (Cell Biolabs Inc., San Diego, CA, USA). Finally, the absorbance was measured at 450 nm and the amount of cAMP was calculated using a cAMP standard curve.

2.9. Reverse transcription-polymerase chain reaction (RT-PCR)

B16F10 melanoma cells were seeded at 1×10^4 cells/mL in 6-well plates and pretreated with α-MSH (500 ng/mL) for 24 h before treatment with pinostrobin (0–50 μM) for 48 h. Total RNA was extracted using an easy-BLUE Total RNA Extraction Kit (iNtRON Biotechnology, Seongnam, Gyeonggi-do, Republic of Korea), according to the manufacturer's protocol. The sequences of the sense and antisense primers were as follows: tyrosinase (*TYR*) sense 5′-GTCGTCACCCTGAAAATCCTAACT-3′ and antisense 5′-CATCGCATAAAACCTGATGGC-3′. *MITF* sense 5′-CCCGTCTCTGGAAACTTGATCG-3′ and antisense 5′-CTGTACTCTGAGCAGCAGGTC-3′, glyceraldehyde-3-phosphate dehydrogenase (*GAPDH*) sense 5′-AGGTCGGTGTGAACGGATTTG-3′ and antisense 5′-TGTAGACCATGTAGTTGAGGTCA-3′. The PCR products were visualized using ethidium bromide.

2.10. Western blot analysis

B16F10 melanoma cells were seeded at a density of 1×10^4 cell/ml in 6-well plates. The cells were then pretreated with α-MSH (500 ng/ml) for 24 h before treatment with pinostrobin (0–50 μM) for 48 h and subsequently lysed using PRO-PREP lysis buffer (iNtRON Biotechnology). The supernatant was collected, and protein concentrations were measured using Bio-Rad protein assay reagents (Bio-Rad, Hercules, CA, USA). Equal amounts of protein were separated on SDS-polyacrylamide gels, transferred to nitrocellulose membranes (Schleicher & Schuell, Keene, NH, USA), and immunoblotted with specific antibodies. The bound antibodies were detected using an enhanced chemiluminescence plus kit (Thermo Fisher Scientific). Images were visualized and captured using ImageQuant LAS 500 (GE Healthcare Bio-Sciences AB, Uppsala, Sweden).

2.11. Maintenance of zebrafish

AB strain zebrafish were provided by C.H. Kang (Nakdong National Institute of Biological Resources, Sangju, Gyeongsangbuk-do, Republic of Korea) and cultured at 28 ℃ under a 14/10 h light/dark cycle. Zebrafish were handled according to the standard guidelines of the Animal Care and Use Committee of Jeju National University (approval No. 2022-0036). Embryos obtained from natural spawning in embryo medium [(NaCl-34.8 g, KCl-1.6 g, $CaCl_2.2H_2O$-5.8 g, $MgCl_2.6H_2O$-9.78 g) with double-distilled water, pH 7.2]. The media was supplemented with 1% methylene blue at 28 °C.

2.12. Melanogenesis and heart rate in zebrafish

One day post-fertilization (dpf) zebrafish larvae (*n = 20*) were pretreated with PTU (200 μM) for 48 h and then incubated with α-MSH (1 μg/mL) for an additional 24 h. At 4 dpf, the medium was replaced with PTU and α-MSH, and the embryos were treated

with pinostrobin (0–25 μM) for 48 h (at 6 dpf). After anesthetizing zebrafish larvae with 0.02% tricane methanesulfonate, they were mounted in 2% methyl cellulose on a depression slide, and images were collected using an Olympus SZ2-ILST stereomicroscope (Tokyo, Japan). Densitometric analysis was performed using the ImageJ software (National Institutes of Health). The quantification of pigmentation data was calculated as a percentage of untreated zebrafish larvae. In a parallel experiment, heart rate was manually calculated using a stereomicroscope. The results are represented as the average heart rate per minute.

2.13. Statistical analysis

All data in this study represent the mean of triplicate experiments and are expressed as mean ± standard error (SE). Statistical analysis was performed using Sigma plot software (version 12.0) by Student's *t*-test and unpaired one-way analysis of variance (ANOVA) with Bonferroni's correction.

3. Results

3.1. Pinostrobin inhibits in vitro mushroom tyrosinase activity

As tyrosinase is a rate-limiting enzyme in melanogenesis [11, 12], we investigated whether pinostrobin negatively regulates mushroom tyrosinase activity in vitro. As expected, tyrosinase inhibitors PTU, AA, and KA significantly inhibited mushroom tyrosinase activity by 74.7% ± 0.6%, 63.8% ±1.0%, and 67.4% ± 0.6%, respectively (Fig. 1B). Meanwhile, as the concentration of pinostrobin gradually increased, in vitro mushroom tyrosinase activity was inhibited, and 1000 μM pinostrobin exhibited the strongest inhibitory effect (58% ± 0.6%). In addition, the IC50 was confirmed to be 527.7 μM (Fig. 1C). Collectively, these data suggest that pinostrobin directly inhibits tyrosinase activity in vitro.

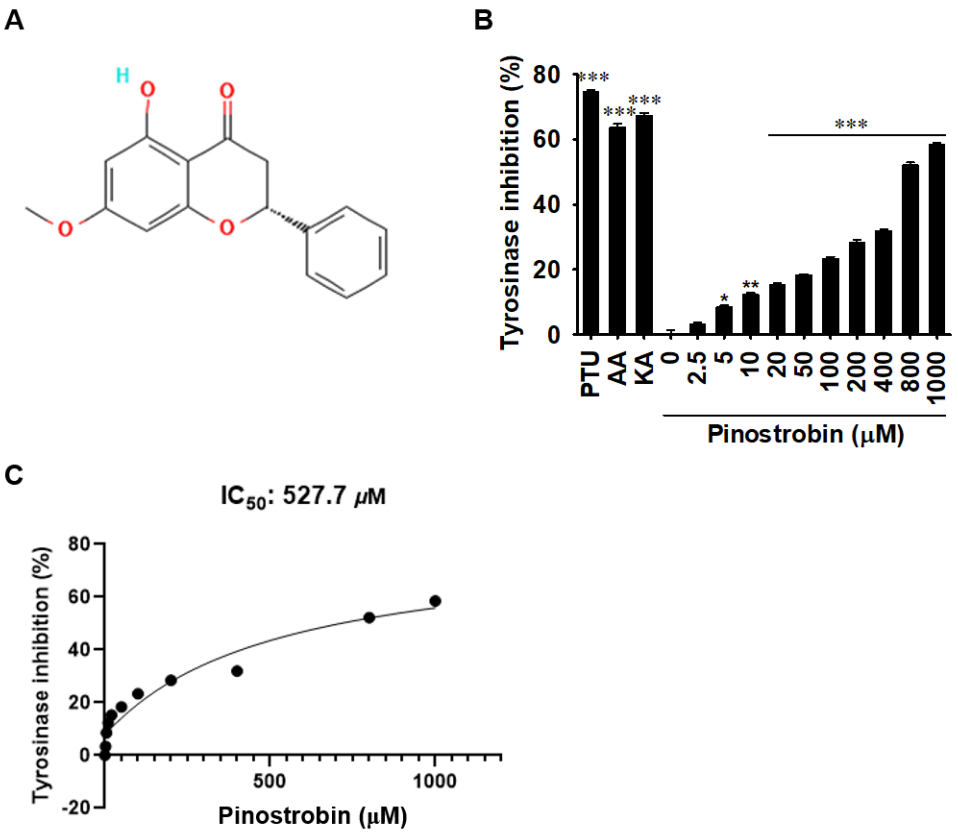

Fig. 1. Pinostrobin inhibits in vitro mushroom tyrosinase activity. (A) Chemical structure of pinostrobin. (B) In vitro mushroom tyrosinase activity, as assessed by quantifying dopaquinone levels, following treatment with pinostrobin (0–1000 μM), PTU (250 nM), ascorbic acid (AA, 500 μM), and kojic acid (KA, 25 μM). Data are reported as the mean ± SE. $^{*}p < 0.05$, $^{**}p < 0.01$, and $^{***}p < 0.001$ vs. untreated control. (C) IC_{50} for pinostrobin.

3.2. Pinostrobin non-competitively binds to tyrosinase

Whether pinostrobin inhibits in vitro mushroom tyrosinase activity by competing with its substrate was analyzed using a protein-ligand docking simulation. Using SwissDock, 36 clusters in which pinostrobin binds to mushroom tyrosinase were identified (Fig. 2A). The major binding site was identified (Fig. 2A 'a'), to which 50% of clusters (0, 1, 3, 4, 8, 13, 17, 20, 21, 22, 23, 24, 27, 28, 30, 34, 35, and 36) were bound. Meanwhile, clusters 2, 6, 9, 14, 18, 19, 31, and 33 were bound to alternative binding site (Fig. 2A 'b'), where the second highest binding force was observed. Additionally, four minor pinostrobin-binding sites were identified (Fig. 2A 'c-f'). The 3D conformation (Fig. 2B) and ribbon structure (Fig. 2C) also showed the major pinostrobin binding site and the active site of tyrosinase containing Cu^{2+} ions. In particular, pinostrobin formed a hydrogen bond with TYR98 (HN) in the light chain (L, lectin-like fold protein) at a distance of 2.4769 Å (Fig. 2D). In addition to the conventional hydrogen bond with TYR98, the 2D interaction diagram showed the formation of carbon hydrogen bonds (THR324), alkyl or π-alkyl bonds (TYR78, ILE324, and PRO338), and many van der Waals interactions with the surrounding amino acids (Fig. 2E). These results indicate that pinostrobin does not compete with substrates at the active site of tyrosinase but rather primarily binds to heavy (H, polyphenol oxidase) and light chains.

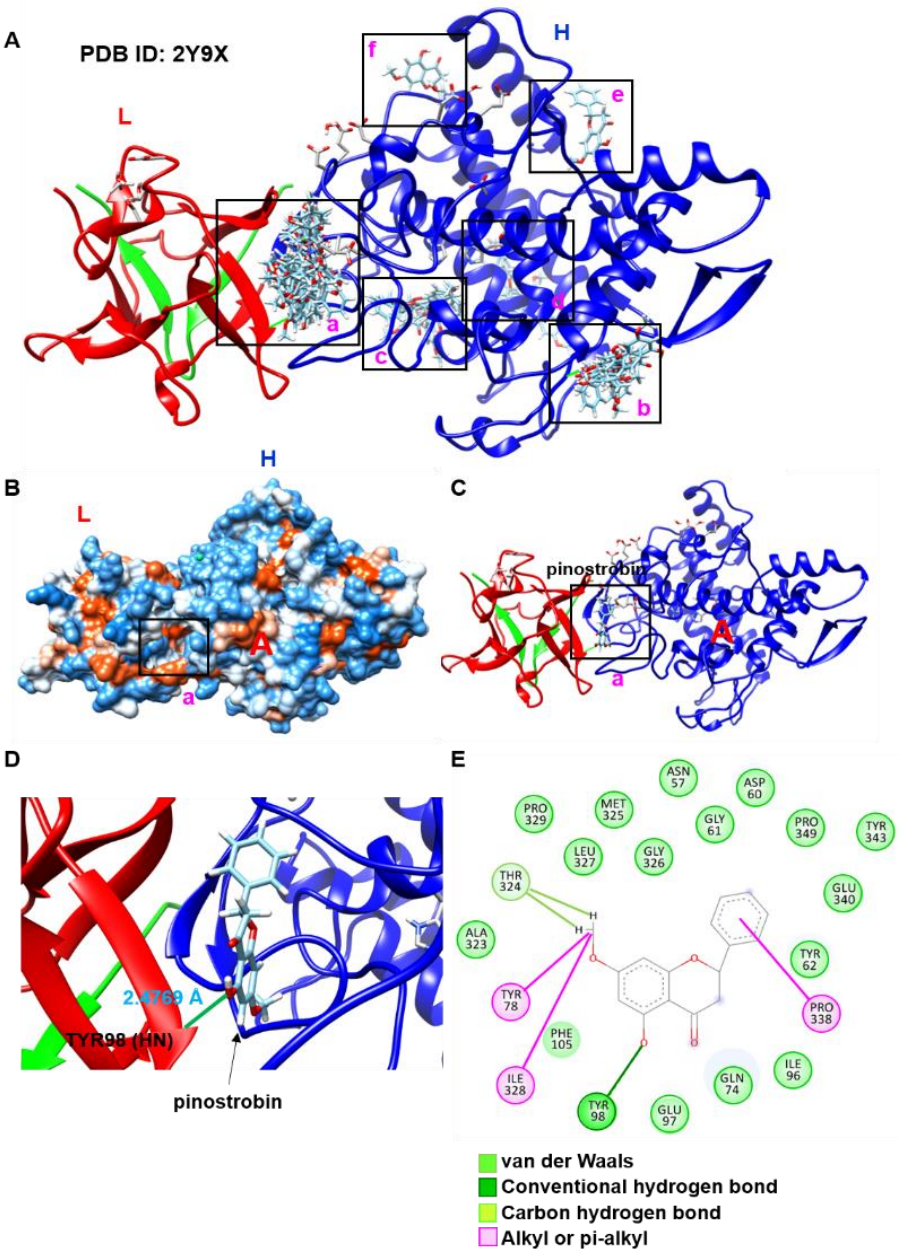

Fig. 2. Pinostrobin non-competitively binds to mushroom tyrosinase (PDB ID: 2Y9X). (A) Total 36 binding clusters of pinostrobin to mushroom tyrosinase were obtained from SwissDock. a binding site for clusters 0, 1, 4, 8, 13, 17, 20, 21, 22, 23, 24, 27, 28, 30, 34, 35, and 36; b, binding site for clusters 2, 6, 9, 14, 18, 19, 31, and 33; c, binding site for clusters 7, 11, 25, 26, 32; d, binding site for clusters 12, 15, and 29; e, binding site for clusters 5 and 16; f, binding site for cluster 10. L, light chain (lectin-like fold protein); H, heavy chain (polyphenol oxidase).

3.3. Pinostrobin concentrations above 100 μM are cytotoxic

To investigate whether pinostrobin is cytotoxic, B16F10 melanoma cells were treated with pinostrobin (0–1000 μM) for 72 h, and cytotoxicity was evaluated based on morphological changes and MTT assay. Observation under a phase-contrast microscope showed that pinostrobin treatment did not induce any morphological changes in the cells (Fig. 3A). However, the MTT assay showed that treatment with pinostrobin at concentrations ≥ 100 μM markedly decreased the relative cell viability after 24 h (77.3% ± 1.0% and 54.3% ± 0.5% at 100 and 200 μM, respectively); the inhibitory effect became stronger after 48 h (68.3% ± 1.1% and 49.2% ± 0.2% at 100 and 200 μM, respectively) and 72 h (39.6% ± 0.1% and 30.6% ± 0.2% at 100 and 200 μM, respectively; Fig. 2B).

To confirm whether pinostrobin influences cell death, flow cytometric analysis was performed (Fig. 1C). Consistent with the MTT assay results, 72 h after pinostrobin treatment, when compared to untreated cells ([3.0 ± 0.2] × 10^6 cells/mL), 100 μM and 200 μM pinostrobin significantly reduced viable cell counts ([1.6 ± 0.1] × 10^6 cells/mL and [1.2 ± 0.6] × 10^6 cells/mL, respectively; Fig. 1D). Moreover, the dead cell population significantly increased to 15.2% ± 0.2% and 20.1% ± 5.6% at 100 and 200 μM pinostrobin, compared to that in untreated cells (7.2% ± 0.3%; Fig. 3E). H_2O_2 treatment for 24 h also significantly decreased viable cell counts (1.6 ± 0.6) × 10^6 cells/mL and increased the dead cell population (23.3% ± 0.2%). However, pinostrobin at concentrations ≤ 50 μM had no effect on cell viability or death. These data indicate that pinostrobin at concentrations below 50 μM has no direct cytotoxic effects.

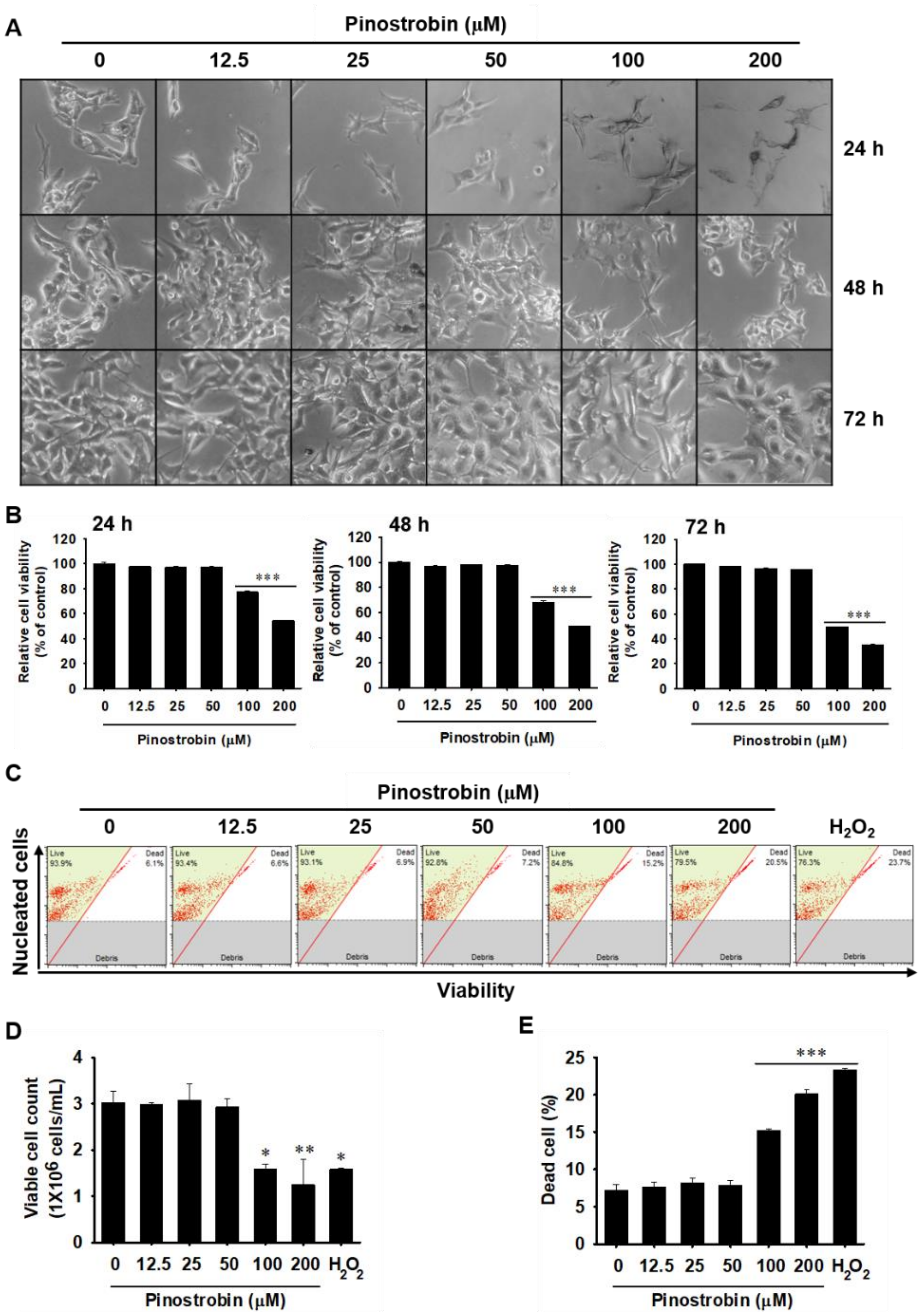

Fig. 3. Pinostrobin at concentrations below 50 μM is not toxic to B16F10 melanoma cells. B16F10 cells were treated with pinostrobin (0–200 μM) for 72 h. (A) Microscopic images captured every 24 h. (B) Relative cell viability presented relative to the values of the untreated cells. (C) Treatment of cells with pinostrobin for 72 h. The cells were stained with a Muse Cell Count & Viability Kit. (D) Viable cell counts; (E) dead cell population Data are reported as mean ± SE. * $p < 0.05$, ** $p < 0.01$, and *** $p < 0.001$ vs. untreated cells.

3.4. Pinostrobin decreases melanin production and intracellular tyrosinase activity

To investigate the anti-melanogenic effect of pinostrobin, α-MSH-stimulated B16F10 melanoma cells were treated with various concentrations of pinostrobin (0–50 μM) for 48 h, and the melanin content was measured in the extracellular and intracellular compartments. The degree of indirect melanin biosynthesis was assessed based on change in media color during cell culture; dark brown color indicates the presence of melanin. Results show a clear increase in melanin following treatment with α-MSH, which gradually decreased upon pinostrobin treatment (Fig. 4A). Additionally, α-MSH significantly increased the extracellular and intracellular melanin contents to approximately 172% (Fig. 4B) and 186% (Fig. 4C), respectively. Meanwhile, pinostrobin downregulated α-MSH-induced extracellular and intracellular melanin content in a concentration-dependent manner. Pinostrobin (50 μM) also decreased α-MSH-induced intracellular tyrosinase activity from approximately 160% to 113% (Fig. 4D). In contrast, the group treated with only 50 μM pinostrobin, without α-MSH pretreatment, exhibited melanin content and tyrosinase activity similar to those of untreated cells. These data indicate that pinostrobin inhibits extracellular and intracellular melanin content, as well as tyrosinase activity.

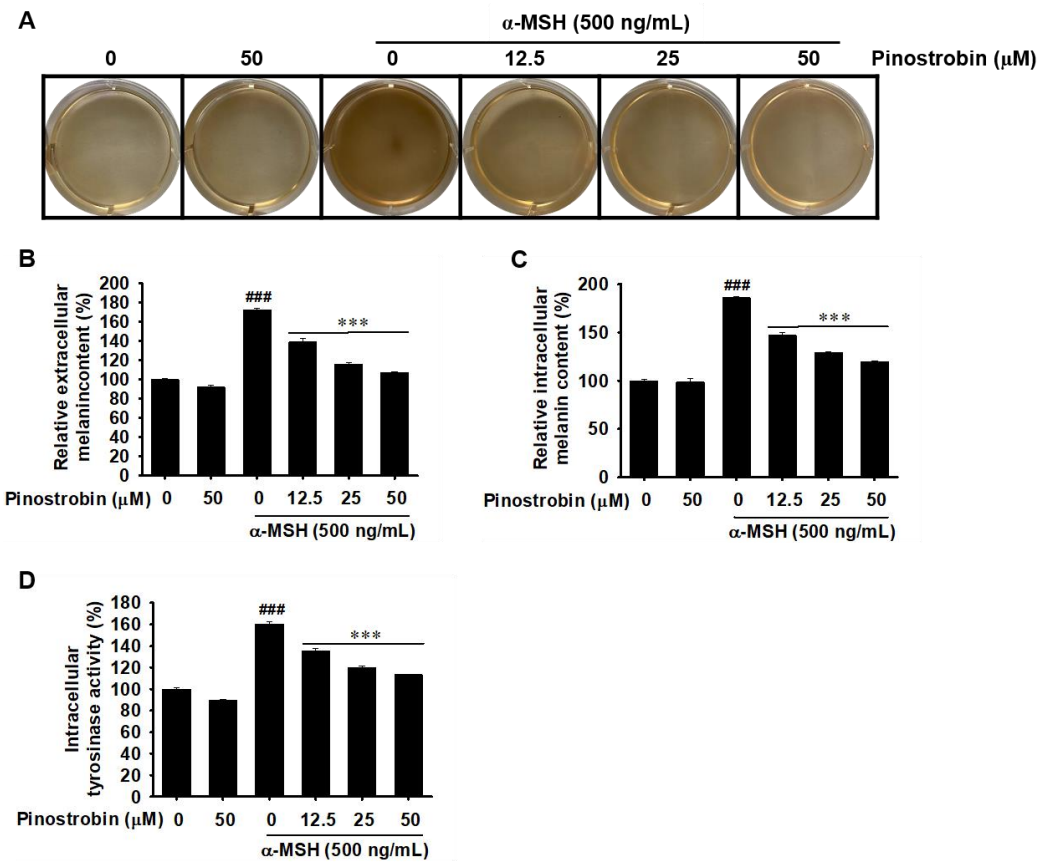

Fig. 4. Pinostrobin decreases α-MSH-stimulated melanin production and intracellular tyrosinase activity. B16F10 cells were stimulated with 500 ng/mL α-MSH for 24 h followed by treatment with pinostrobin (0–50 μM) for 48 h. (A) The color change of each well. (B) Extracellular melanin content following stimulation with or without α-MSH and treatment with pinostrobin. (C) Intracellular melanin content following stimulation with or without α-MSH and treatment with pinostrobin. (D) Intracellular tyrosinase activity following treatment with B16F10 cells with pinostrobin and stimulation with or without α-MSH. The data are represented as mean ± SE. $^{###}$ $p <$ 0.001 vs. untreated cells and *** $p < 0.001$ vs. α-MSH-treated cells.

3.5. Pinostrobin inhibits cAMP, p-CREB, MITF, and tyrosinase expression in α-MSH-stimulated B16F10 melanoma cells

To elucidate the mechanism by which pinostrobin inhibits the α-MSH-induced melanogenic signaling pathway, we measured cAMP levels induced by the binding of α-MSH to MC1R. As shown in Fig. 5A, pinostrobin significantly downregulated the increase in cAMP levels induced by α-MSH from 421.7 ± 14.3 pg/mL to 231.0 ± 21.7 pg/mL, 144.4 ± 5.1 pg/mL, and 96.9 ± 3.4 pg/mL at 12.5, 25, and 50 μM, respectively. Considering that upregulation of intracellular cAMP is directly associated with CREB phosphorylation, we also evaluated the effect of pinostrobin on CREB phosphorylation. α-MSH markedly increased the expression of phosphorylated CREB (p-CREB), whereas pinostrobin decreased p-CREB expression in a concentration-dependent manner (Fig. 5B). Additionally, α-MSH noticeably upregulated MITF and tyrosinase at both the translational (Fig. 5C) and transcriptional (Fig. 5D) levels whereas pinostrobin reduced α-MSH-induced MITF and tyrosinase expression at both levels. These results indicate that pinostrobin inhibits the melanogenic signaling pathway by suppressing the **cAMP-CREB-MITF-**tyrosinase axis.

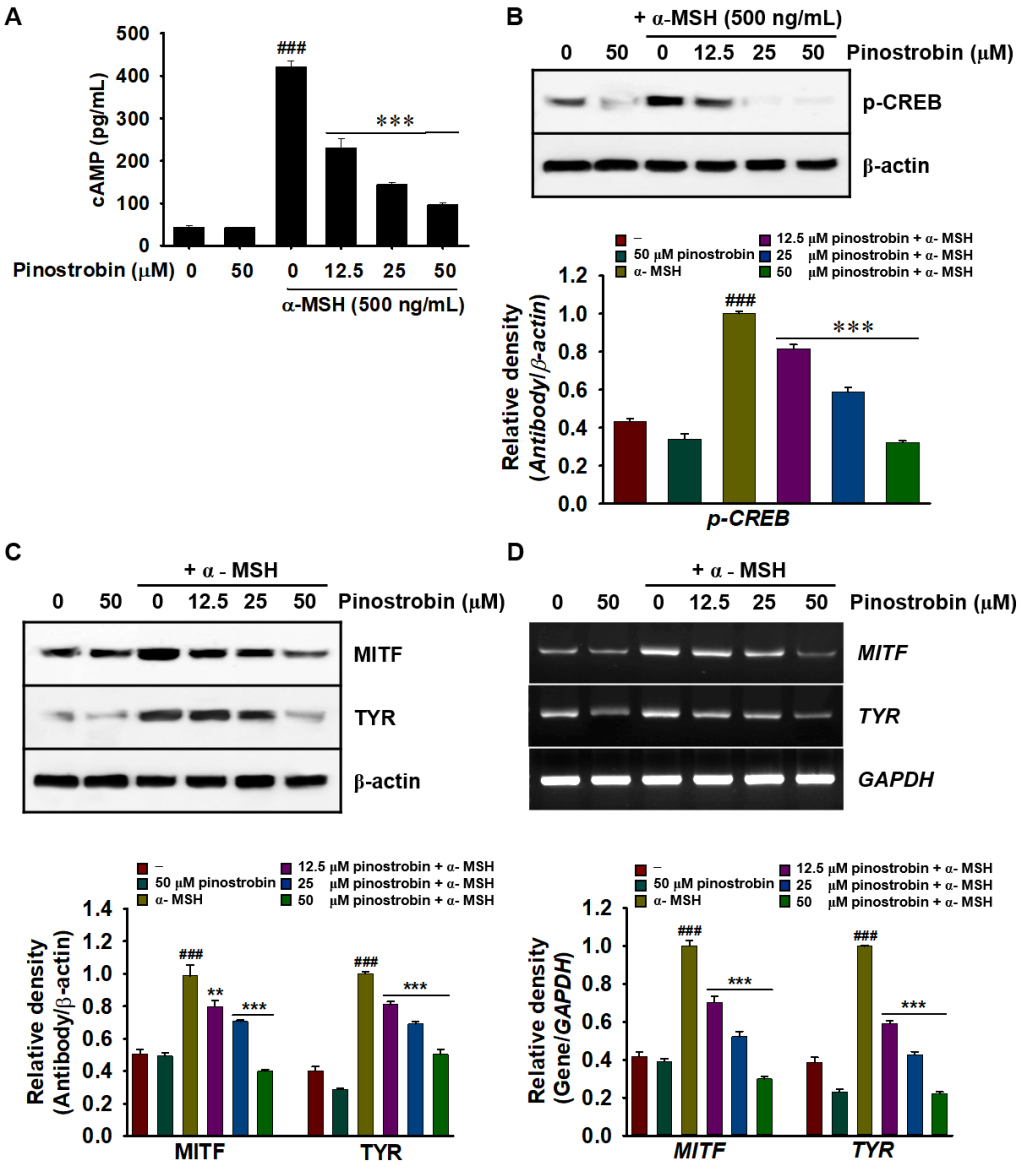

Fig. 5. Pinostrobin inhibits α-MSH-induced melanogenic signaling pathway. (A) Intracellular cAMP levels of B16F10 melanoma cells following pretreatment with BMX for 10 min and treatment with pinostrobin in the presence or absence of **α**-MSH. (B and C) Protein abundance of p-CREB, MITF, and tyrosinase (TYR) in B16F10 melanoma cells exposed α-MSH and subsequently treated with pinostrobin. (D) Expression of *MITF* and *tyrosinase* in B16F10 melanoma cells exposure to α-MSH and subsequently treated with pinostrobin. The data are represented as mean ± SE. $^{###}$ $p<$ 0.001 vs. untreated cells** $p < 0.01$ and *** $p < 0.001$ vs. α-MSH-stimulated cells.

3.6. Pinostrobin inhibits melanin biosynthesis in zebrafish larvae

To further evaluate the anti-melanogenic activity of pinostrobin, we treated α-MSH-stimulated zebrafish larvae with pinostrobin and quantified subsequent melanogenesis. As expected, pinostrobin markedly decreased α-MSH-induced melanin pigmentation in zebrafish larvae in a concentration-dependent manner (Fig. 6A). Pinostrobin at 25 μM inhibited α-MSH-induced melanin pigmentation in untreated zebrafish larvae (Fig. 6B). To determine whether pinostrobin exerted cardiotoxicity in zebrafish larvae, we monitored the heart rate and found that zebrafish larvae treated with pinostrobin did not show any apparent difference compared to that in the untreated larvae (Fig. 6C). Furthermore, neither morphological malformations nor mortality of the larvae were observed following treatment with pinostrobin for 48 h (data not shown). These results suggest that pinostrobin is also a potent inhibitor of melanogenesis in vivo.

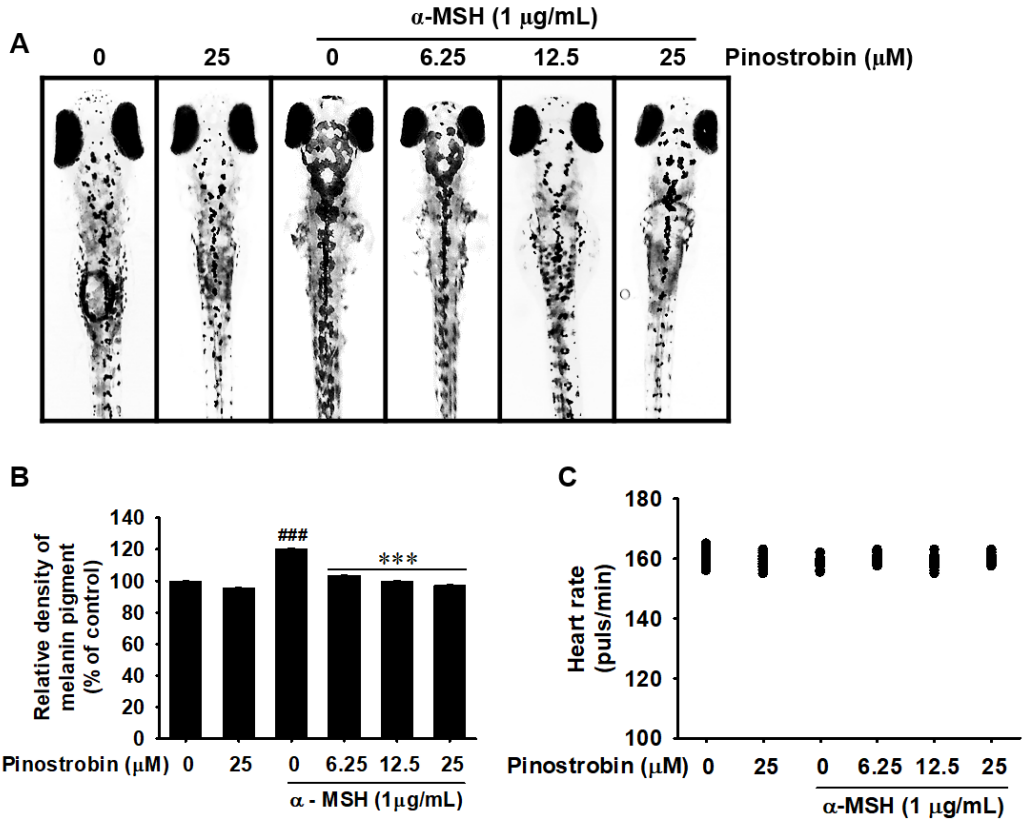

Fig. 6. Pinostrobin inhibits melanin biosynthesis in zebrafish larvae. (A and B) Zebrafish larvae at 2 dpf treated with PTU (200 μM) and stimulated with α-MSH (1 μg/ml). (A) Microscopic evaluation of zebrafish larvae pigmentation (40×). (B) Relative melanin pigment density. (C) Average heart rate of zebrafish larvae (n = 20). Data are reported as the mean ± SE. $^{###}$ $p < 0.001$ vs. untreated zebrafish larvae; *** $p < 0.001$ vs. α-MSH-stimulated zebrafish larvae.

4. Discussion

UV exposure promotes α-MSH expression in keratinocytes, which stimulates the melanogenic signaling pathway by binding to MC1R in melanocytes [1, 2]. The melanin produced by melanocytes spreads to the epidermis via keratinocytes and protects cells against UV-induced ROS stress and apoptosis [3, 4]. However, abnormal hyperpigmentation creates skin darkness, such as spots or patches, by increasing melanin production when skin cells are severely damaged [24]. In addition to skin injury, accumulated melanin also induces acquired hyperpigmentation disorders, including metabolic, endocrine, and nutritional disorders [25]. Therefore, many drugs that can effectively inhibit tyrosinase activity with few side effects have been developed and are currently being used in clinical practice [26]. In this respect, many flavonoids that target tyrosinase have been evaluated [20]. Although several previous studies demonstrated that pinostrobin inhibits tyrosinase activity in vitro [20, 27], the exact molecular mechanism has not been studied. In this study, we investigated that pinostrobin inhibits direct tyrosinase activity and α-MSH-induced melanogenic activity.

Tyrosinase is a rate-limiting enzyme for melanin biosynthesis and contains copper ions at the catalytic center, which catalyze the hydroxylation and oxidation of substrates, including L-tyrosine and L-DOPA, to form dopachrome, resulting in melanin biosynthesis [28]. Therefore, many inhibitors targeting the catalytic center in tyrosinase have been developed [10, 29, 30]. In particular, many natural flavonoids fit into the catalytic pocket and are suitable chelators of Cu^{2+} using a flavonoid core and ionizable OH substituents. Hence, many flavonoids inhibit tyrosinase activity by competing with substrates at their catalytic site [31-33]. In this study, we demonstrated that pinostrobin inhibits mushroom tyrosinase activity in vitro; with an IC_{50} higher than that of

flavonoids previously reported in other studies [34, 35]. Molecular docking simulation confirmed the binding site of pinostrobin in tyrosinase. Unlike previously known flavonoids, pinostrobin does not fit into the active and catalytic centers, but rather binds primarily to another site between the light chain (lectin-like fold protein) and heavy chain (polyphenol oxidase). Whether this binding induces a conformational change in tyrosinase and acts as a non-competitive inhibitor is currently unknown. However, it is clear that binding inhibits the activity of mushroom tyrosinase in vitro.

Numerous cell-signaling pathways are also involved in melanin biosynthesis. Among these, α-MSH-mediated upregulation of MITF is considered a key inducer of melanogenesis [36]. The binding of α-MSH to MC1R promotes cAMP formation and subsequently activates PKA-mediated CREB phosphorylation, which consequently transactivates MITF [14]. Activated MITF subsequently enhances the transcription of melanogenesis-related proteins such as tyrosinase [37]. Liu-Smith and Meyskens [38] previously reported that flavonoids inhibit melanin biosynthesis by suppressing the cAMP-PKA-CREB-MITF-tyrosinase signaling pathway, leading to excellent effects in the prevention and treatment of melanoma via the suppression of melanin production. In this study, we found that pinostrobin effectively inhibited α-MSH-mediated melanin biosynthesis, both in vitro and in vivo, by suppressing tyrosinase expression and activity. Unlike previous studies [34, 39], pinostrobin effectively inhibits melanin biosynthesis in α-MSH-treated B16F10 melanoma cells and zebrafish larvae at 50 and 25 μM, respectively, which is relatively low compared with the IC50 (527.2 μM) of in vitro mushroom tyrosinase. These results suggest that pinostrobin exerts its effect predominantly via interference with the melanin biosynthesis cell signaling pathway rather than through direct inhibition of tyrosinase activity. Additionally, Pillaiyar et al. [40] reported that several soluble factors, such as wingless-related integration site, stem

cell factor, and endothelin-1, stimulate MITF-mediated melanogenesis in melanocytes. Therefore, it is necessary to determine whether pinostrobin also contributes to the inhibition of other signaling pathways in addition to inhibiting the α-MSH-induced melanogenesis signaling process.

In conclusion, this study demonstrates that pinostrobin potently inhibits melanin biosynthesis in vitro and in vivo, thus eliciting a significant anti-melanogenic effect. This suggests that pinostrobin has the potential for novel clinical applications in the prevention and treatment of dermatological disorders, including wrinkling, melasma, and senile lentigines.

References

[1] Cichorek M, Wachulska M, Stasiewicz A, Tyminska A. Skin melanocytes: Biology and development. Postepy Dermatol Alergol. 2013;30:30-41.

[2] Ohbayashi N, Fukuda M. Recent advances in understanding the molecular basis of melanogenesis in melanocytes. F1000Res. 2020;9.

[3] Solano F. Photoprotection and skin pigmentation: Melanin-related molecules and some other new agents obtained from natural sources. Molecules. 2020;25.

[4] Napolitano A, Panzella L, Monfrecola G, d'Ischia M. Pheomelanin-induced oxidative stress: Bright and dark chemistry bridging red hair phenotype and melanoma. Pigment Cell Melanoma Res. 2014;27:721-33.

[5] Cestari TF, Dantas LP, Boza JC. Acquired hyperpigmentations. An Bras Dermatol. 2014;89:11-25.

[6] Fistarol SK, Itin PH. Disorders of pigmentation. J Dtsch Dermatol Ges. 2010;8:187-201; quiz -2.

[7] Goelzer Neto CF, do Nascimento P, da Silveira VC, de Mattos ABN, Bertol CD. Natural sources of melanogenic inhibitors: A systematic review. Int J Cosmet Sci. 2022;44:143-53.

[8] Qian W, Liu W, Zhu D, Cao Y, Tang A, Gong G, et al. Natural skin-whitening compounds for the treatment of melanogenesis (Review). Exp Ther Med. 2020;20:173-85.

[9] Noh H, Lee SJ, Jo HJ, Choi HW, Hong S, Kong KH. Histidine residues at the copper-binding site in human tyrosinase are essential for its catalytic activities. J Enzyme Inhib Med Chem. 2020;35:726-32.

[10] Goldfeder M, Kanteev M, Isaschar-Ovdat S, Adir N, Fishman A. Determination of tyrosinase substrate-binding modes reveals mechanistic differences between

type-3 copper proteins. Nat Commun. 2014;5:4505.

[11] Sohretoglu D, Sari S, Barut B, Ozel A. Tyrosinase inhibition by some flavonoids: Inhibitory activity, mechanism by in vitro and in silico studies. Bioorg Chem. 2018;81:168-74.

[12] Nazir Y, Rafique H, Roshan S, Shamas S, Ashraf Z, Rafiq M, et al. Molecular docking, synthesis, and tyrosinase inhibition activity of acetophenone amide: Potential inhibitor of melanogenesis. Biomed Res Int. 2022;2022:1040693.

[13] Oren M, Bartek J. The sunny side of p53. Cell. 2007;128:826-8.

[14] Garcia-Borron JC, Abdel-Malek Z, Jimenez-Cervantes C. MC1R, the cAMP pathway, and the response to solar UV: extending the horizon beyond pigmentation. Pigment Cell Melanoma Res. 2014;27:699-720.

[15] Zhou S, Zeng H, Huang J, Lei L, Tong X, Li S, et al. Epigenetic regulation of melanogenesis. Ageing Res Rev. 2021;69:101349.

[16] Jones AA, Gehler S. Acacetin and pinostrobin inhibit malignant breast epithelial cell adhesion and focal adhesion formation to attenuate cell migration. Integr Cancer Ther. 2020;19:1534735420918945.

[17] Jadaun A, Sharma S, Verma R, Dixit A. Pinostrobin inhibits proliferation and induces apoptosis in cancer stem-like cells through a reactive oxygen species-dependent mechanism. RSC Adv. 2019;9:12097-109.

[18] Wu N, Fu K, Fu YJ, Zu YG, Chang FR, Chen YH, et al. Antioxidant activities of extracts and main components of Pigeonpea [*Cajanus cajan* (L.) Millsp.] leaves. Molecules. 2009;14:1032-43.

[19] Bahadur Gurung A, Ajmal Ali M, Al-Hemaid F, El-Zaidy M, Lee J. In silico analyses of major active constituents of fingerroot (*Boesenbergia rotunda*) unveils inhibitory activities against SARS-CoV-2 main protease enzyme. Saudi J

Biol Sci. 2022;29:65-74.

[20] El-Nashar HAS, El-Din MIG, Hritcu L, Eldahshan OA. Insights on the inhibitory power of flavonoids on tyrosinase activity: A survey from 2016 to 2021. Molecules. 2021;26.

[21] Duckworth HW, Coleman JE. Physicochemical and kinetic properties of mushroom tyrosinase. J Biol Chem. 1970;245:1613-25.

[22] Bitencourt-Ferreira G, de Azevedo WF, Jr. Docking with SwissDock. Methods Mol Biol. 2019;2053:189-202.

[23] Chung S, Lim GJ, Lee JY. Quantitative analysis of melanin content in a three-dimensional melanoma cell culture. Sci Rep. 2019;9:780.

[24] Lee AY. Skin pigmentation abnormalities and their possible relationship with skin aging. Int J Mol Sci. 2021;22.

[25] Yamaguchi Y, Hearing VJ. Melanocytes and their diseases. Cold Spring Harb Perspect Med. 2014;4.

[26] Zolghadri S, Bahrami A, Hassan Khan MT, Munoz-Munoz J, Garcia-Molina F, Garcia-Canovas F, et al. A comprehensive review on tyrosinase inhibitors. J Enzyme Inhib Med Chem. 2019;34:279-309.

[27] Patel NK, Jaiswal G, Bhutani KK. A review on biological sources, chemistry and pharmacological activities of pinostrobin. Nat Prod Res. 2016;30:2017-27.

[28] Solano F. On the metal cofactor in the tyrosinase family. Int J Mol Sci. 2018;19.

[29] Rolff M, Schottenheim J, Decker H, Tuczek F. Copper-O_2 reactivity of tyrosinase models towards external monophenolic substrates: molecular mechanism and comparison with the enzyme. Chem Soc Rev. 2011;40:4077-98.

[30] Favre E, Daina A, Carrupt PA, Nurisso A. Modeling the met form of human tyrosinase: A refined and hydrated pocket for antagonist design. Chem Biol Drug

Des. 2014;84:206-15.

[31] Jakimiuk K, Sari S, Milewski R, Supuran CT, Sohretoglu D, Tomczyk M. Flavonoids as tyrosinase inhibitors in in silico and in vitro models: basic framework of SAR using a statistical modelling approach. J Enzyme Inhib Med Chem. 2022;37:421-30.

[32] Arroo RRJ, Sari S, Barut B, Ozel A, Ruparelia KC, Sohretoglu D. Flavones as tyrosinase inhibitors: Kinetic studies in vitro and in silico. Phytochem Anal. 2020;31:314-21.

[33] Li X, Guo J, Lian J, Gao F, Khan AJ, Wang T, et al. Molecular simulation study on the interaction between tyrosinase and flavonoids froms sea buckthorn. ACS Omega. 2021;6:21579-85.

[34] Obaid RJ, Mughal EU, Naeem N, Sadiq A, Alsantali RI, Jassas RS, et al. Natural and synthetic flavonoid derivatives as new potential tyrosinase inhibitors: A systematic review. RSC Adv. 2021;11:22159-98.

[35] Promden W, Viriyabancha W, Monthakantirat O, Umehara K, Noguchi H, De-Eknamkul W. Correlation between the potency of flavonoids on mushroom tyrosinase inhibitory activity and melanin synthesis in melanocytes. Molecules. 2018;23.

[36] Kawakami A, Fisher DE. The master role of microphthalmia-associated transcription factor in melanocyte and melanoma biology. Lab Invest. 2017;97:649-56.

[37] Hida T, Kamiya T, Kawakami A, Ogino J, Sohma H, Uhara H, et al. Elucidation of melanogenesis cascade for identifying pathophysiology and therapeutic approach of pigmentary disorders and melanoma. Int J Mol Sci. 2020;21.

[38] Liu-Smith F, Meyskens FL. Molecular mechanisms of flavonoids in melanin

synthesis and the potential for the prevention and treatment of melanoma. Mol Nutr Food Res. 2016;60:1264-74.

[39] Abbas Q, Ashraf Z, Hassan M, Nadeem H, Latif M, Afzal S, et al. Development of highly potent melanogenesis inhibitor by in vitro, in vivo and computational studies. Drug Des Devel Ther. 2017;11:2029-46.

[40] Pillaiyar T, Manickam M, Jung SH. Recent development of signaling pathways inhibitors of melanogenesis. Cell Signal. 2017;40:99-115.